Taher Abu Ali, M.Eng

Fabrication and poling of ferroelectric composites

MASTER'S THESIS

to achieve the university degree of

Diplom-Ingenieur

Master's degree programme:

Advanced Materials Science

submitted to

Graz University of Technology

Supervisor

Assoc. Prof. Dr. Anna Maria Coclite

Co-supervisor

Univ.-Prof. Ph.D. Peter Hadley

Institute of Solid State Physics

Graz, August 2018

AFFIDAVIT

I declare that I have authored this thesis independently, that I have not used other than the declared sources/resources, and that I have explicitly indicated all material which has been quoted either literally or by content from the sources used.
The text document uploaded to TUGRAZonline is identical to the present master‘s thesis dissertation.

Date Signature

……. …….....

Acknowledgement

For starters, I would like to sincerely thank Dr. Jonas Groten, for his support and thorough supervision during the time spent at Joanneum Research. I would also like to thank the PyzoFlex research team, which consists of Dr. Martin Zirkl, Dr. Maria Belegratis, Mag. Philipp Schäffner, DI Andreas Tschepp , Eng. Michael Suppan for their assistance with the measurements and characterization techniques. Moreover, special thanks goes to the Hybrid electronics research group leader Dr. Barbara Stadlober.

Apart from Joanneum Research, I would like to express my appreciation for the guidance obtained from my academic supervisor Anna Maria Coclite. Guidance, which helped in successfully completing this master thesis. Additionally, I would like to thank professor Peter Hadley for his role in arranging the thesis position at Joanneum Research.

In the end, I would like to express my deepest love, appreciation and gratitude to my parents and siblings for their continuous support throughout this journey. Thank you, I owe it all to you!

Abstract

This thesis deals with the development of a pressure and temperature sensing technology based on ferroelectric nanocomposite material. Both pyroelectric and piezoelectric properties of the ferroelectric nanocomposite are utilized. The nanocomposite material consists of a P(VDF-TrFE) matrix phase and a ceramic nanoparticles phase. In a single phase material based on ferroelectric PVDF copolymers, both pyroelectric and piezoelectric effects are simultaneously utilized, which translates to simultaneous temperature and pressure sensing respectively. Therefore, thermal contributions during pressure sensing as well as vibration effects during temperature sensing are present. However, the proposed nanocomposite material allows separate poling of it constituents by controlling the poling direction (parallel or antiparallel poling of phases). Since the polymer matrix phase has a negative pyroelectric coefficient p and a negative piezoelectric coefficient d_{33}, while the nanoparticle phase has a negative pyroelectric coefficient and a positive piezoelectric coefficient, poling both phases opposite to each other would eliminate the effective pyroelectric response of the nanocomposite material and thus control thermal drifts arising during pressure sensing. On the other hand, poling both phases in the same direction, would eliminate the effective piezoelectric response and thus control vibration effects influencing the measured temperature.

Two nanocomposite materials are investigated in this thesis, the 1st material is based on P(VDF-TrFE) 70:30 mol-% matrix phase and Lead Titanite (PT) 20 vol-% filler phase. The 2nd material presented, which provides an environmental-friendly as well as biocompatible lead-free nanocomposite material, is composed of P(VDF-TrFE) 70:30 mol-% matrix phase and Bismuth Sodium Titanite (BNT) 20 vol-% filler phase.

Preparation of the samples using a cheap, reliable and efficient screen printing technique, which allows industrialized production of these sensors for commercial use, is presented as well in this thesis. The presented technology is used to print the nanocomposite material into a parallel plate structure with a thickness *t* of 7 µm, with PEDOT:PSS electrodes being printed using the same screen printing technique.

In the results section, DC poling of the nanoparticle phase is presented, where P(VDF-TrFE)-PT nanocomposite exhibits a measured pyroelectric coefficient of 11.9 µC/Km^2 in comparison to 4.3 µC/Km^2 for P(VDF-TrFE)-BNT nanocomposite. However, *D-E* hysteresis loops obtained for both materials from AC poling of the matrix phase show that for P(VDF-

TrFE)-BNT nanocomposite material, a remnant displacement value of 58 mC/m^2 is measured in comparison to 38 mC/m^2 for P(VDF-TrFE)-PT nanocomposite. Pyroelectric as well as piezoelectric signal cancellation based on separate poling of both nanocomposite phases is presented for both materials.

Table of Contents

List of figures

List of tables

1. Introduction

1.1 Dielectrics:

Dielectric materials are insulators, which conduct no electrical current. By applying an external electrical field, the dielectric material is polarized. Moreover, dielectric materials undergo change in dimensions upon exposure to an external electric field. This can be explained by the displacement of positive and negative charges within the material, which are bound chemically together. The cations are displaced in the direction of the applied electrical field, while anions are displaced in the opposite direction. This displacement results in material deformation and thus changes in dimensions [1].

While the dielectric polarization vanishes after removing the electric field (materials with centrosymmetric crystals), some materials sustain polarization after the field is removed (materials with non-centrosymmetric crystals). Additionally, in ferroelectric materials, spontaneous polarization is present due to structural changes related to paraelectric-ferroelectric phase transition. In case of crystalline materials 11 out of the 32 crystal classes (corresponding to 32 crystallographic point groups), have a center of symmetry and are classified as centrosymmetric [2]. Due to the center of symmetry, the net deformation in the crystal is nonexistent in an ideal case. The remaining 21 crystal classes have no center of symmetry and are classified as non-centrosymmetric. Due to the lack of symmetry center, the ions will displace asymmetrically resulting in significant deformation, which is directly proportional to the external electric field. The lack of center of symmetry gives rise to several physical effects, such as pyroelectric, piezoelectric and ferroelectric effects. Figure 1 gives a clear classification of dielectric materials [1].

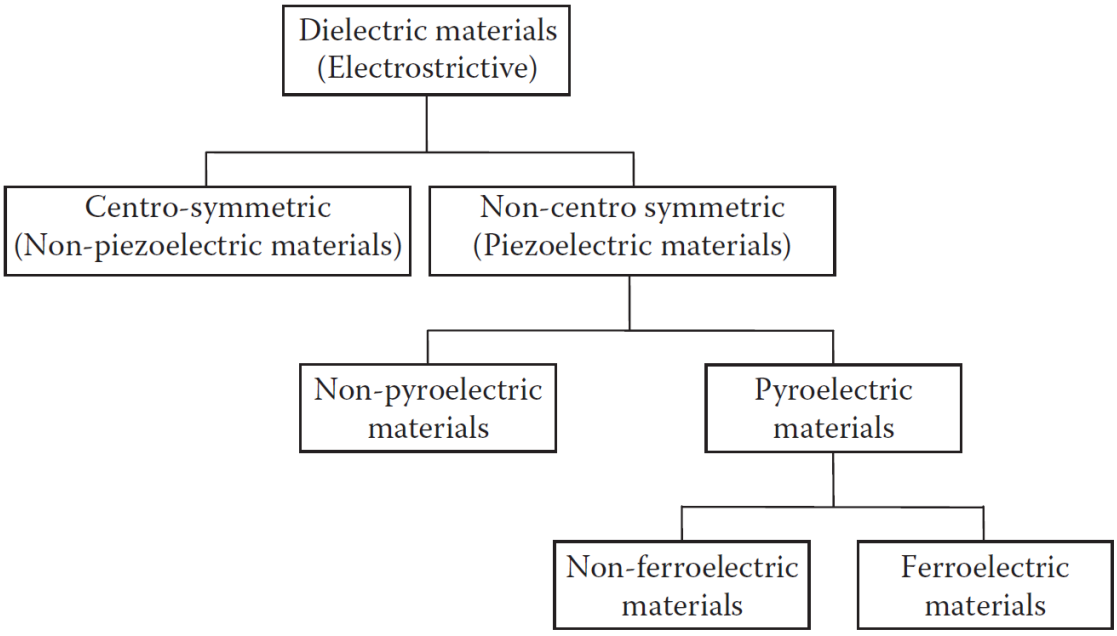

Figure 1-classification of dielectric materials [1]

1.2 Parameters of dielectric materials:

An electric dipole moment is generated inside an atom/molecule, when the centers of positive and negative charges are separated by a distance *d* as shown in figure 2. The electric dipole moment *p* is given by

$$\vec{p} = q\vec{d} \qquad (1.1)$$

Where *q* is the charge and *d* is the separation distance between positive and negative charges.

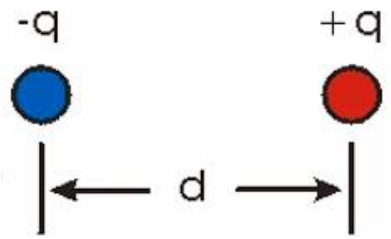

Figure 2-dipole moment dependent on charge separation q and distance d [11]

Dielectric materials can be classified as polar and nonpolar. Atoms/molecules in nonpolar dielectric materials do not have spontaneous dipole moments, as the centers of positive and negative charges overlap. Under an external electric field, electric dipoles are generated but vanish as soon as the field is removed. However, atoms/molecules in polar dielectric materials have spontaneous dipole moments, as the centers of positive and negative charges do not overlap. Under an external electric field, electric dipoles are oriented in the direction of the field (figure 3) [1].

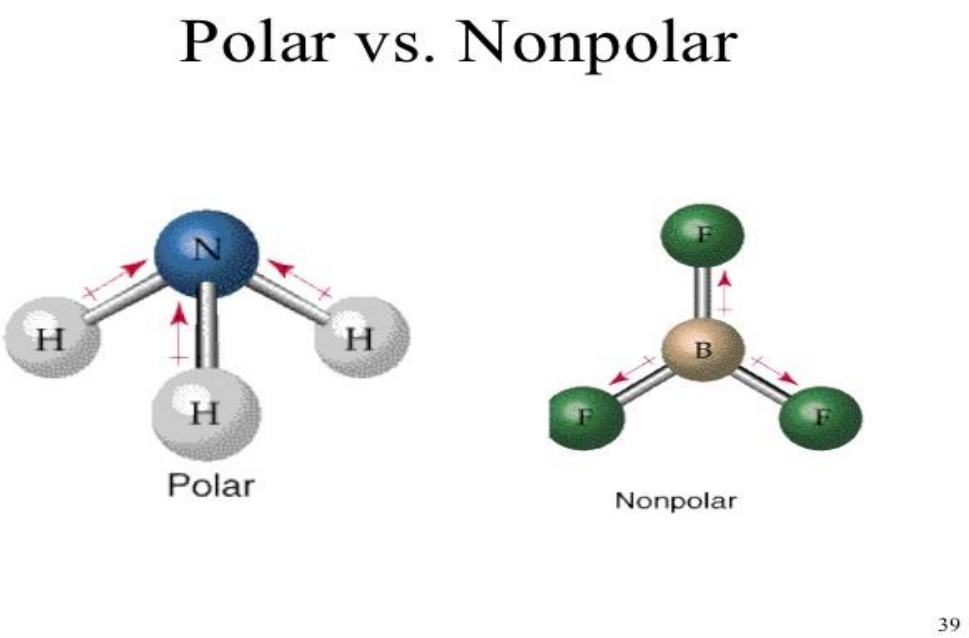

Figure 3-polar vs nonpolar dielectrics [4]

A polar dielectric material consists of a large number of atoms or molecules each possessing an electric dipole moment. The total dipole moment of the dielectric material is the sum of all the single dipole moments given by equation 1.2

$$\sum_i \vec{p}_i \qquad (1.2)$$

Electric polarization *P* is defined as the total dipole moment per unit volume and is given by equation 1.3

$$\vec{P} = \frac{\sum_i \vec{p}_i}{V} \qquad (1.3)$$

Usually, the single dipole moments in a polar dielectric material are randomly oriented, which results in a zero net polarization. Under an external electric field, the single dipole moments arrange in the direction of the electric field. This results in a net polarization, which increases with increased electric field, until saturation (arrangement of all individual dipole moments) is reached [1].

As previously mentioned, under an applied electric field *E*, dielectric materials produce a polarization *P*. Polar materials will show orientation polarization while nonpolar materials will show induced polarization. The electric displacement *D* developed inside the material is given by equation (1.4)

$$\vec{D} = \varepsilon_0 \vec{E} + \vec{P} \qquad (1.4)$$

Where ε_0 is the vacuum permittivity.

D can also be expressed by

$$\vec{D} = \varepsilon_r \varepsilon_0 \vec{E} \qquad (1.5)$$

Where $\varepsilon_r$is the relative permittivity or the dielectric constant.

The polarization *P* is directly related to the applied electric field and is given by equation (1.6)

$$\vec{P} = X \varepsilon_0 \vec{E} \qquad (1.6)$$

Where *X* is the electric susceptibility.

Pyroelectric and ferroelectric materials are characterized by the presence of spontaneous polarization P_s, which drops in value as temperature increases. Moreover, the spontaneous polarization can be switched in direction and increased in magnitude (Poling).

2. Theory

2.1 Piezoelectricity:

Based on the classification in figure 1, dielectric materials with no center of symmetry are classified as piezoelectric materials. In case of crystalline materials exhibiting piezoelectricity, the asymmetric displacement of anions and cations inside the crystal is significant under an external electric field, which results in strain directly proportional to the electric field *E*. Whereas for polymers exhibiting piezoelectricity, such as PVDF, which are composed of crystallites embedded in an amorphous matrix (Small ordered β-phase regions with ideal polymer chain alignment). When compressed or stretched the distance of between these crystallites is changed, resulting in a change of dipole density, and thus in change of macroscopic polarization. The deformation (strain) can be compressive or extensive, a factor influenced by the polarity of the applied field. This effect is referred to as the indirect piezoelectric effect (figure 4). If a pressure/stress is applied on a piezoelectric material, then strain is induced. Induced strain is a result of electric dipoles orientation in the strained crystal, which results in an electrical field across the crystal. This effect is the direct piezoelectric effect (figure 5) [1].

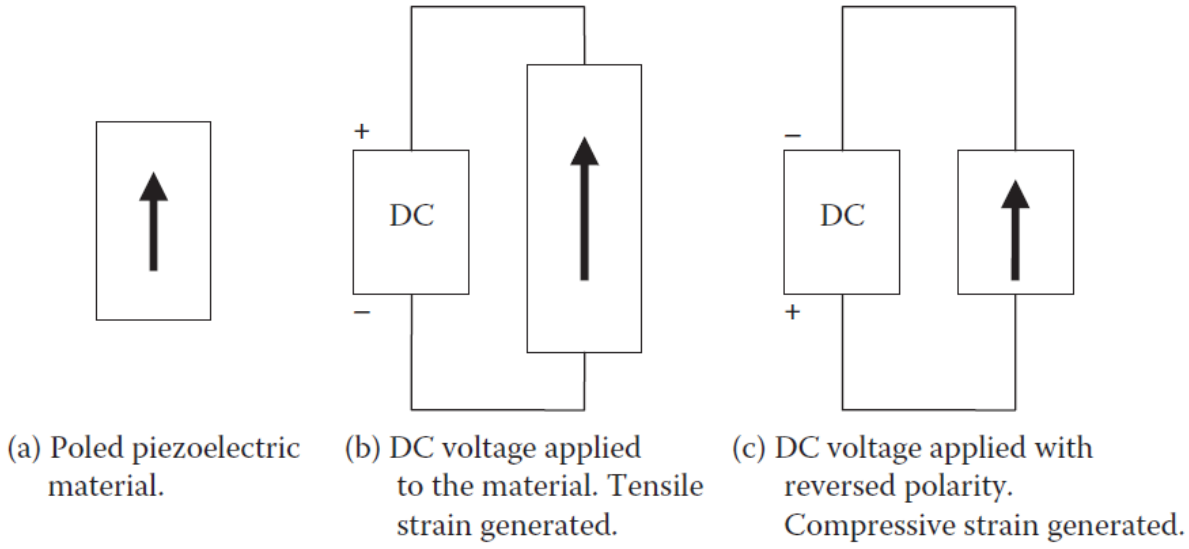

Figure 4-Indirect piezoelectric effect under applied external field [1]

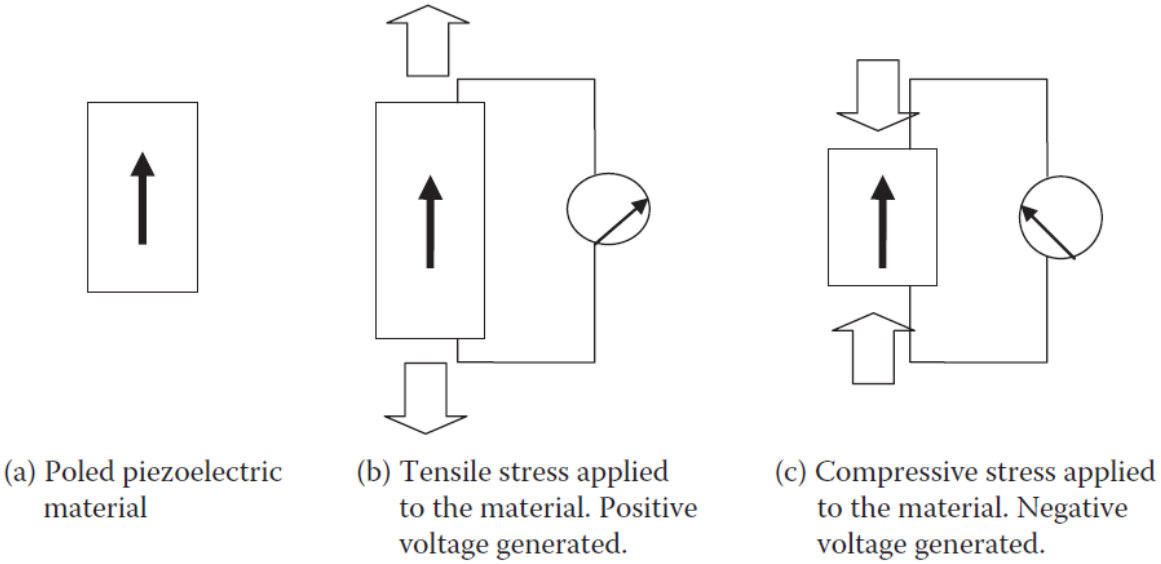

Figure 5-direct piezoelectric effect: induced strain generates voltage [1]

When an external AC electric field is applied to a piezoelectric material, then the material is expected to contract and expand at the same frequency of the applied field (figure 6).

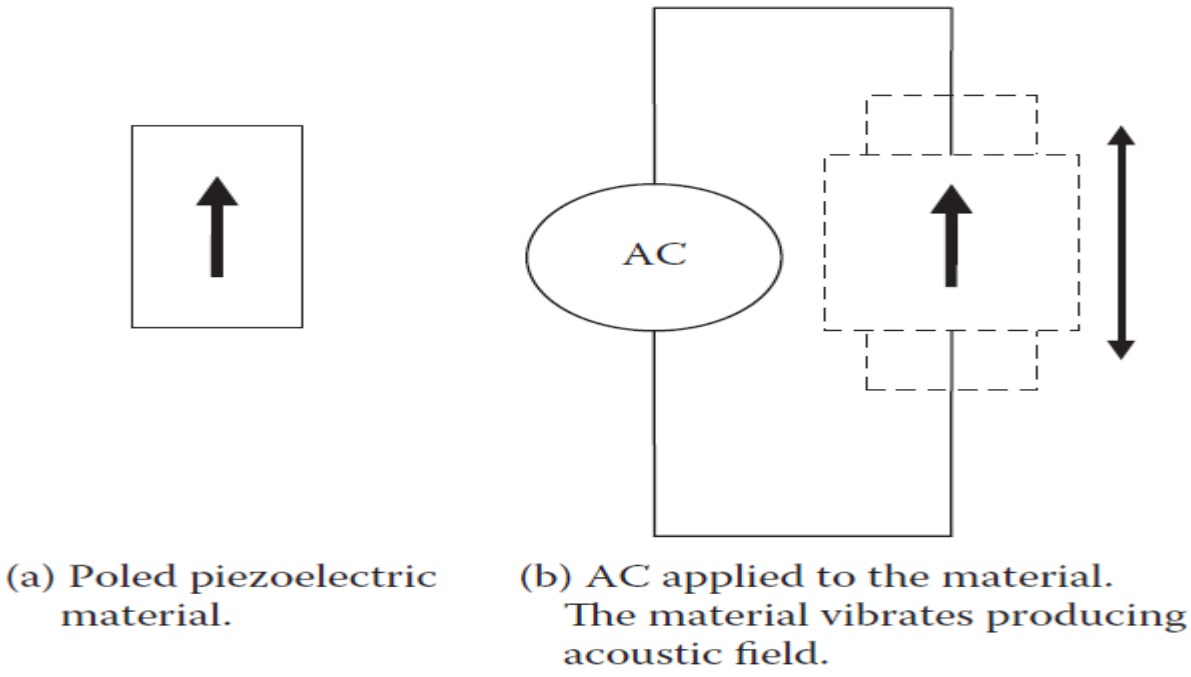

Figure 6-Piezoelectric material's behavior under AC field [1]

2.2 Piezoelectric coupling equations:

Under low electric fields or mechanical stresses, piezoelectric materials show linear behavior. However, a nonlinear behavior is expected under high electric fields or mechanical stresses. The linear behavior of piezoelectric materials is the base for the electromechanical equations used to describe the piezoelectric effect [3].

The electrochemical equations for linear piezoelectric materials is given by equations 2.1 and 2.2

$$\varepsilon_{ij} = S_{ijmk}\sigma_k + d_{mik}E_m \qquad (2.1)$$

$$D_m = d_{mij}\sigma_{ij} + \varepsilon_{mk}E \qquad (2.2)$$

Where the indices *i*, *j*= 1, 2,…, 6 and *m*, *k*= 1, 2, 3 are different directions within the coordinate system of the material. The equations can also be written in the following form

$$\varepsilon_{ij} = S_{ij}\sigma_j + g_{ijm}D_m \qquad (2.3)$$

$$E_i = g_{ikm}\sigma_{km} + \beta_{ik}D \qquad (2.4)$$

Where

σ is the stress tensor

ε is the strain tensor

E is the applied electric field

ε is the permittivity

d is the piezoelectric strain constants matrix

S is the compliance coefficients matrix

D is electric displacement vector

g is the piezoelectric constants matrix

β is the impermitivity component

Of particular relevance is the piezoelectric strain constant d_{mi}, which is described as the ratio of developed free strain to the applied electric field.

2.3 Pyroelectricity:

Pyroelectric materials are polar materials with spontaneous polarization P_s. According to the textbook of Hellwege, a ferroelectric material is a pyroelectric material whose polarization can be reversed, indicating that polarization of pyroelectric materials cannot be reversed [6]. Usually, depositing or contacting two electrodes to the pyroelectric material will allow current flow due to change in surface charge density related to change in spontaneous polarization. When a pyroelectric material is heated, the spontaneous polarization decreases and the change is measured. A mathematical description is given by equation (2.5)

$$dP_s = -pdT \qquad (2.5)$$

Where p is the pyroelectric coefficient (vector) and dT is the change in temperature. The Spontaneous polarization P_s (vector) drops with increased temperature and is indicated by the negative sign. Ferroelectric materials (subclass of pyroelectric materials) exhibit higher pyroelectric activity compared to non-ferroelectric materials, which are discussed in the next subsection of this chapter [1].

2.4 Ferroelectricity:

A ferroelectric material is a material with permanent electric dipole moment, and is named in analogy to ferromagnetic materials, which possess a permanent magnetic dipole moment [5]. Ferroelectric materials are a subclass of pyroelectric materials, which in turn are a subclass of piezoelectric materials, or materials with no center of symmetry. Similar to pyroelectric materials, ferroelectric materials exhibit spontaneous polarization P_s. In ferroelectric materials, the spontaneous polarization can be reversed, unlike pyroelectric materials [1]. In addition to the spontaneous polarization and the ability to reverse it, ferroelectric materials have the following characteristics:

- Ferroelectric hysteresis
- Phase transition above a certain temperature called Curie temperature
- The polarization P has a nonlinear dependency to the applied electric field E

2.5 Characteristics of ferroelectric materials:

Ferroelectric materials are characterized by the presence of ferroelectric domains. Ferroelectric domains are microscopic regions within the material, where all electric dipoles are oriented in the same direction. A ferroelectric material is composed of a large number of domains, which are randomly oriented to yield a net polarization of zero [6]. Applying an electrical field (Poling) orients the domains and increasing the electric field would align all the domains into one single domain (Ideal case). The behavior of ferroelectric materials under applied electric field shows a hysteresis behavior as shown in figure 7.

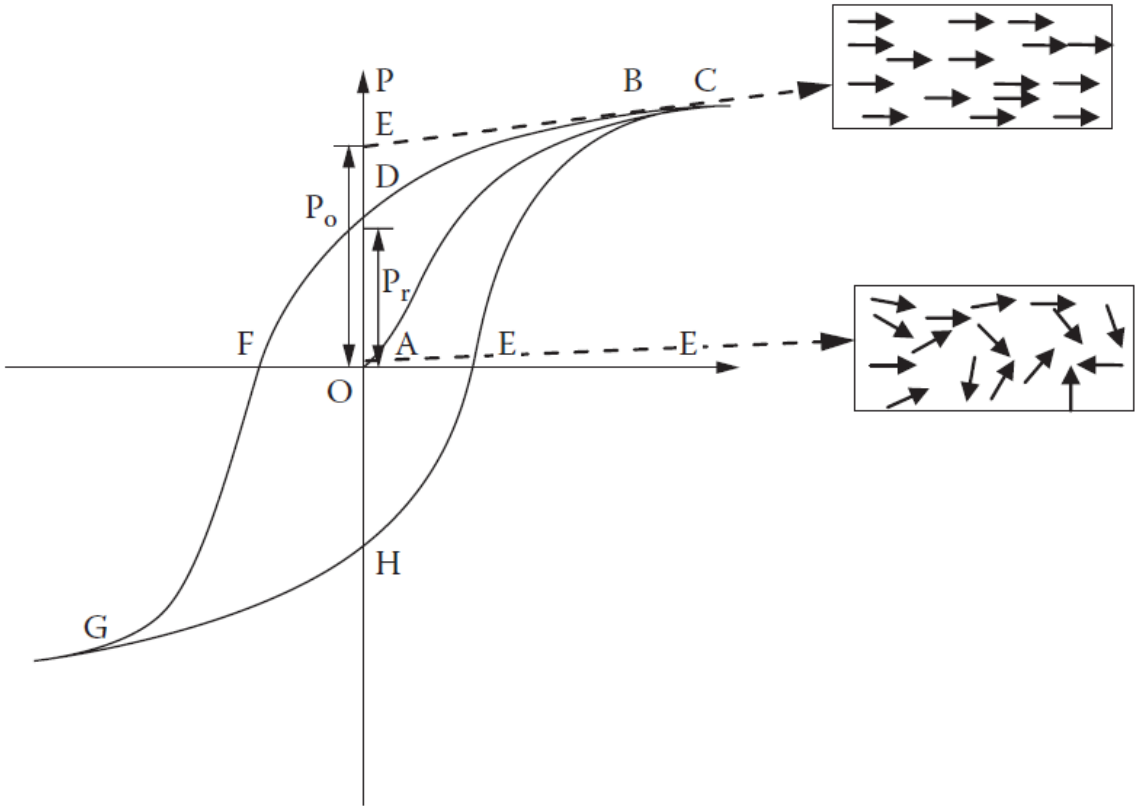

Figure 7-typical ferroelectric P-E hysteresis curve [1]

Point O shows an initial net polarization of 0, due to the absence of an electric field. As the electric field is increased, the domains start to orient in the same direction and a net polarization is obtained. The behavior at this stage is linear, as shown in segment OA of the curve. A nonlinear behavior is realized when the electric field is increased further. When all domains are oriented, a saturation polarization is reached P_0 (point B). Reducing the electric field gradually results in polarization drop, as shown in segment BD. When the field is reduced to zero, ferroelectric materials still attain polarization called remnant polarization P_r, segment OD. To

remove the remnant polarization, an electric field in the opposite direction must be applied. The polarization drops to zero at an electric field called the coercive field E_C, point F. If the field is increased above the coercive field value, a negative saturation polarization -$P_0$is obtained. If the field is reduced to zero, then the curve will have a negative remnant polarization -P_r (Point H). If the field is increased beyond the coercive field E_C, the polarization will follow the path HB until the loop is closed. Such ferroelectric loop is called a hysteresis loop [1].

Ferroelectric materials are characterized by a transition temperature called the Curie temperature T_c. Above the Curie temperature, the ferroelectric material loses its spontaneous polarization and transitions into the paraelectric phase [5]. The paraelectric phase does not show any hysteresis response to the applied electric field E and maintains no remnant polarization $P_r$when the field vanishes (figure 8).

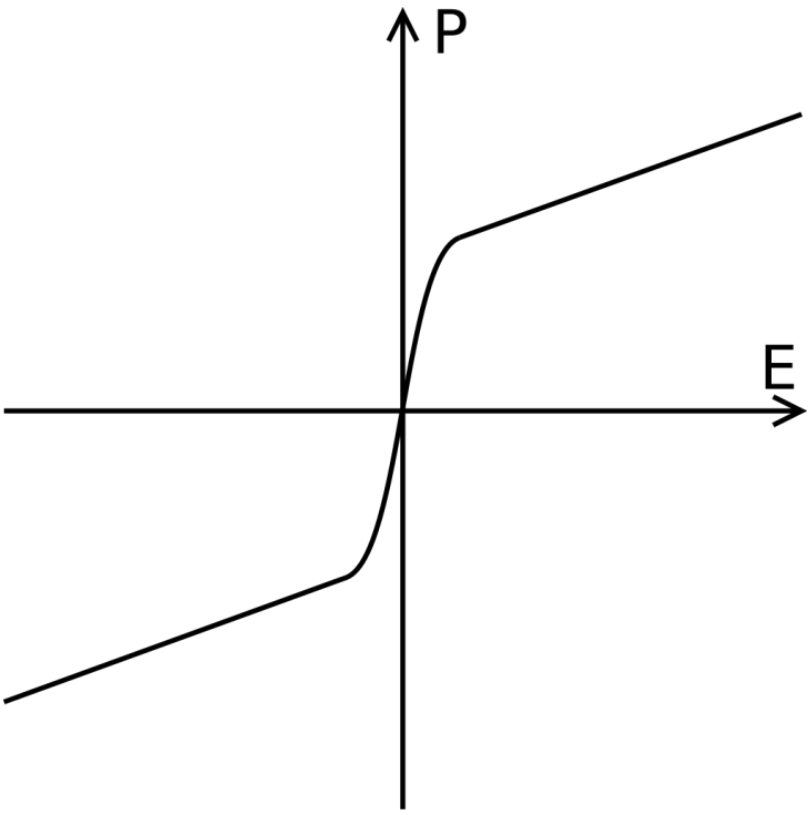

Figure 8-paraelectric phase behavior under external electrical field [7]

2.6 Polyvinylidene fluoride:

Ferroelectric polymers have been a topic of investigation for the past decades. Most notably known ferroelectric polymer is polyvinylidene fluoride (PVDF) and it's copolymers. PVDF is used for pressure and temperature sensing which relies on its superior pyroelectric and piezoelectric properties associated with its ferroelectric nature.

PVDF is obtained from polymerization of Vinylidene fluoride, which has a chemical formula CH_2CF_2 (Figure 9). The repeating Vinylidene fluoride unit has a vacuum dipole moment p of 7×10^{-30} Cm [12] and is formed by the positive hydrogen atoms and the negative fluoride atoms. The hydrogen and fluoride atoms are attached to the main carbon chain, which limits their orientation to the molecular conformation. Due to the different molecular conformations, several PVDF polymorphs exist. A conformation of particular interest is the all-trans conformation, which translates to ferroelectric β-phase. β-phase PVDF and the other polymorphs will be discussed in the coming subsection [8].

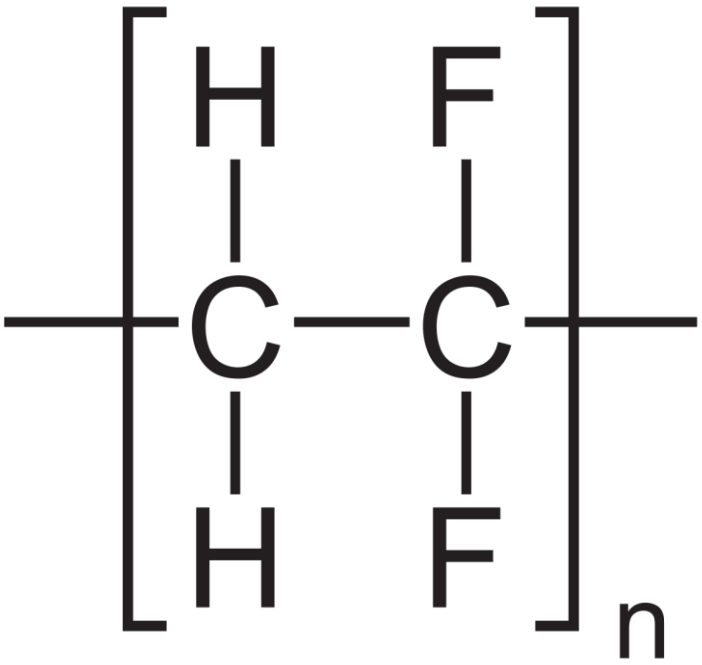

Figure 9-PVDF chemical formula indicates that it is a fluorinated polymer [12]

2.6.1 Polymorphs:

Although β-phase PVDF is very useful for its ferroelectric properties, it is not the most common nor the most stable polymorph. β-phase PVDF is one of four polymorphs, in which paraelectric α-phase PVDF is the most stable polymorph. α-phase PVDF follows a TGTG conformation as shown in figure 10, which is characterized by a nonpolar crystal structure [12].

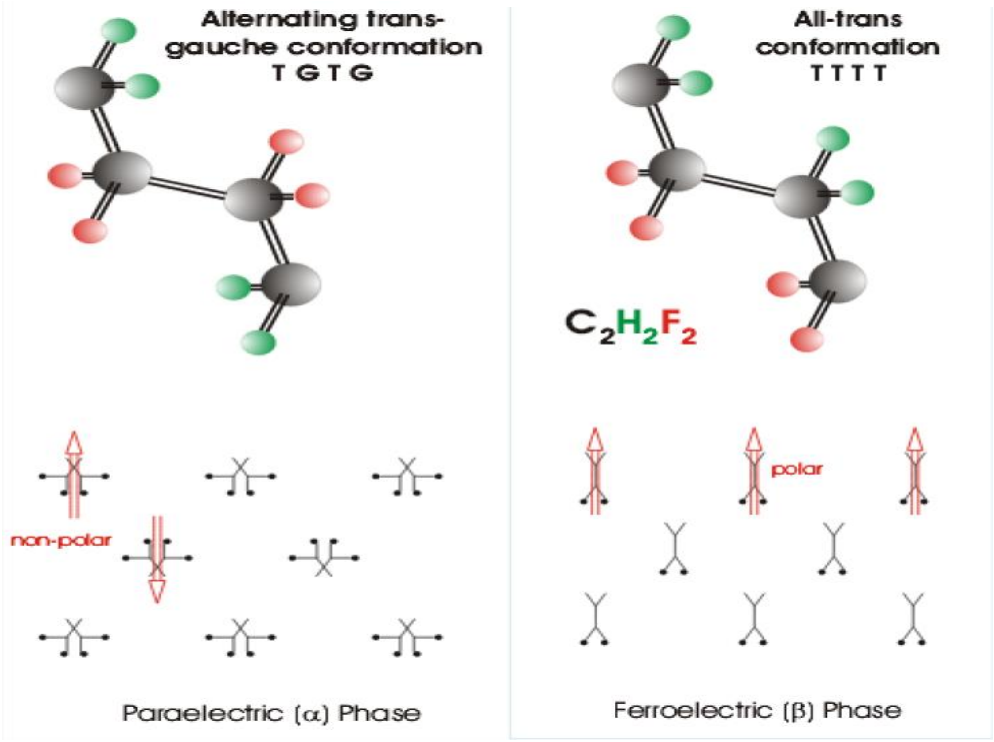

Figure 10-trans-gauche conformation verses all-trans conformation [9]

Direct crystallization from the melt produces α-phase PVDF, which can be easily converted into ferroelectric β-phase PVDF by mechanical drawing or annealing of α-phase PVDF under high temperature and pressure. β-phase PVDF follows an all-trans TTTT conformation as seen in figure 9. If α-phase PVDF is heated and annealed at elevated temperature then the process induces transformation into an intermediate γ-phase, which unlike α-phase PVDF is polar and more stable at high temperatures. With the application of high electric field, α-phase PVDF is transformed into δ-phase, which is also polar. Figure 11 shows the four different polymorphs and how to obtain one from the other [8].

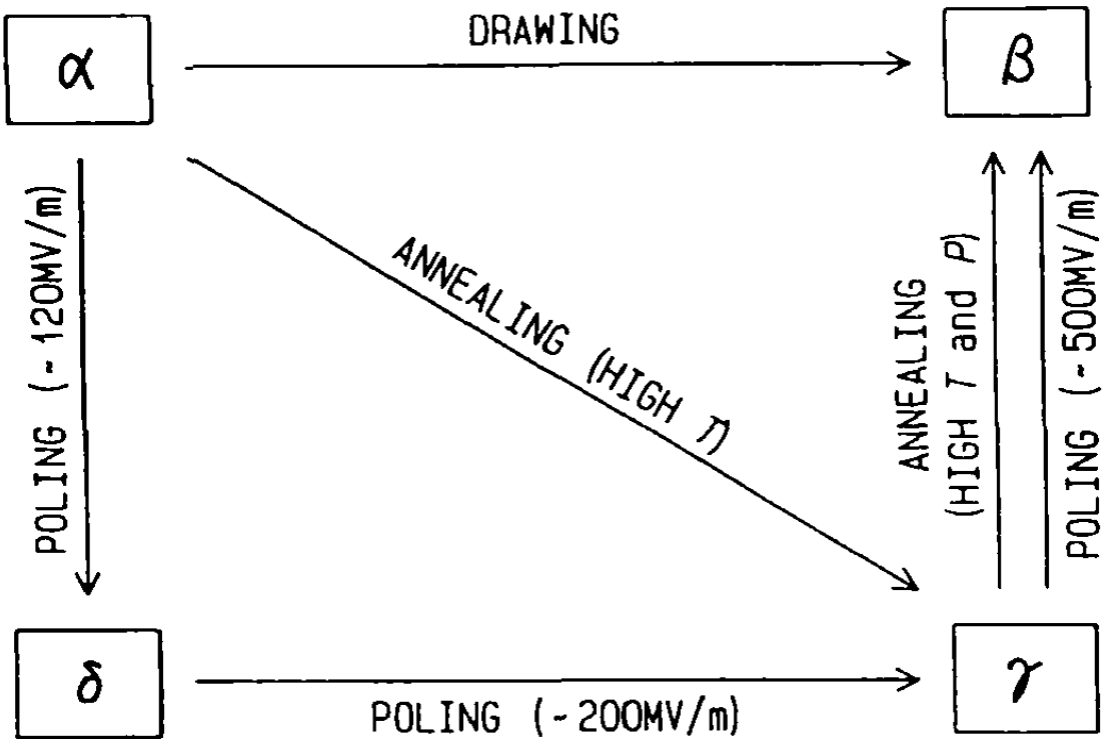

Figure 11-PVDF polymorphs and how to obtain them [8]

2.6.2 Copolymers:

As mentioned previously, crystallization from the melt results in the formation of paraelectric α-phase PVDF. In order to obtain the desired ferroelectric β-phase PVDF, mechanical drawing or annealing under high pressure and temperature has to be employed. However, it was discovered that the addition of trifluoroethylene (TrFE) into PVDF would actually enhance the formation of the β-phase directly from the melt. In addition to enhancing the formation of β-phase directly from the melt, The crystallinity increased up to 90% depending on the VDF to TrFE ratio, on contrary to pure PVDF which has a crystallinity degree of about 50% to 70% [8][10]. Since piezoelectricity and pyroelectricity depend on the crystallinity of the material, then an increase in the crystallinity degree would result in improved piezoelectric and pyroelectric signals. Moreover, higher remnant polarization P_r is obtained. Another advantage of VDF copolymerization with TrFE is that the resultant copolymer would have a defined Curie temperature T_C, a characteristic that is missing from pure PVDF [10]. The Curie temperature depends on the TrFE content. 70:30 mol-% P(VDF-TrFE) has a Curie temperature of around 105°C. However, 80:20 mol-% P(VDF-TrFE) has a Curie temperature of around 145°C. These numbers indicate that the Curie temperature of the copolymer increases with decreased TrFE content. The chemical structure of P(VDF-TrFE) is shown in figure 12.

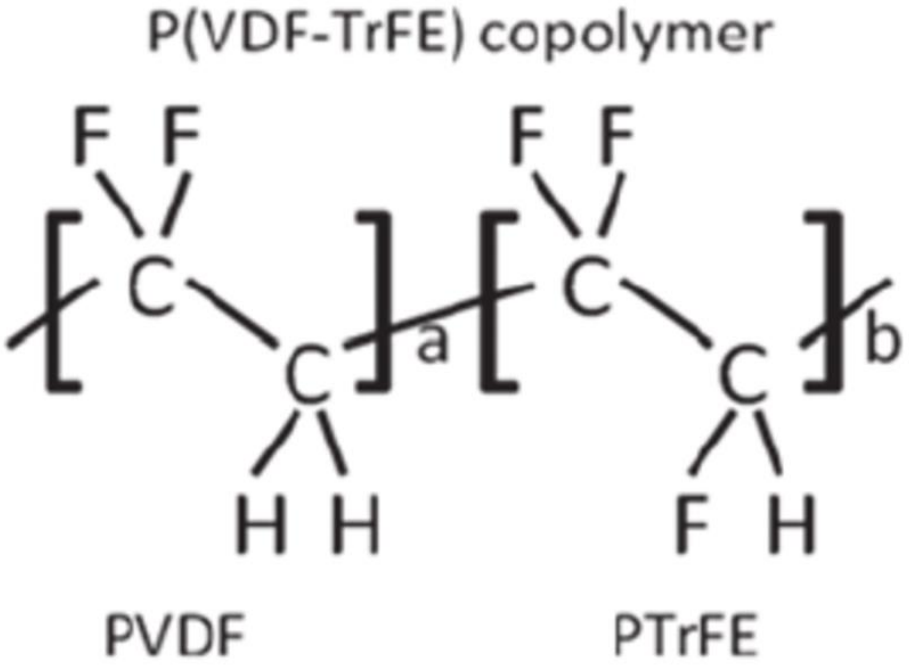

Figure 12-Chemical structure of P(VDF-TrFE) consisting of one VDF unit and TrFE unit [10]

2.6.3 Ferroelectric properties of PVDF:

A poling procedure would be essential to obtain high remnant polarization. Previously, poling of PVDF was done by applying a relatively low electric field at elevated temperature for long poling times. Typical field value is around 30 MV/m, poling temperature of around 100 °C and poling time of roughly 30 minutes. However, the resultant remnant polarization was notably low. However it was later observed, that much higher electric fields are required and that poling must be done at a low temperature (around room temperature) in order to obtain a significant remnant polarization [8].

To observe the ferroelectric properties of PVDF, *D-E* hysteresis loops are generated, an example of a *D-E* hysteresis loop for PVDF is shown in figure 13. The *D-E* curve is measured at 20°C, with a frequency *f*=1 Hz and by applying a high AC field. As seen in the figure , below the coercive field E_C, the remnant displacement is very low. However, once the coercive field value of 50 MV/m has been exceeded, a much higher displacement/remnant polarization is obtained, around 60 mC/m^2.

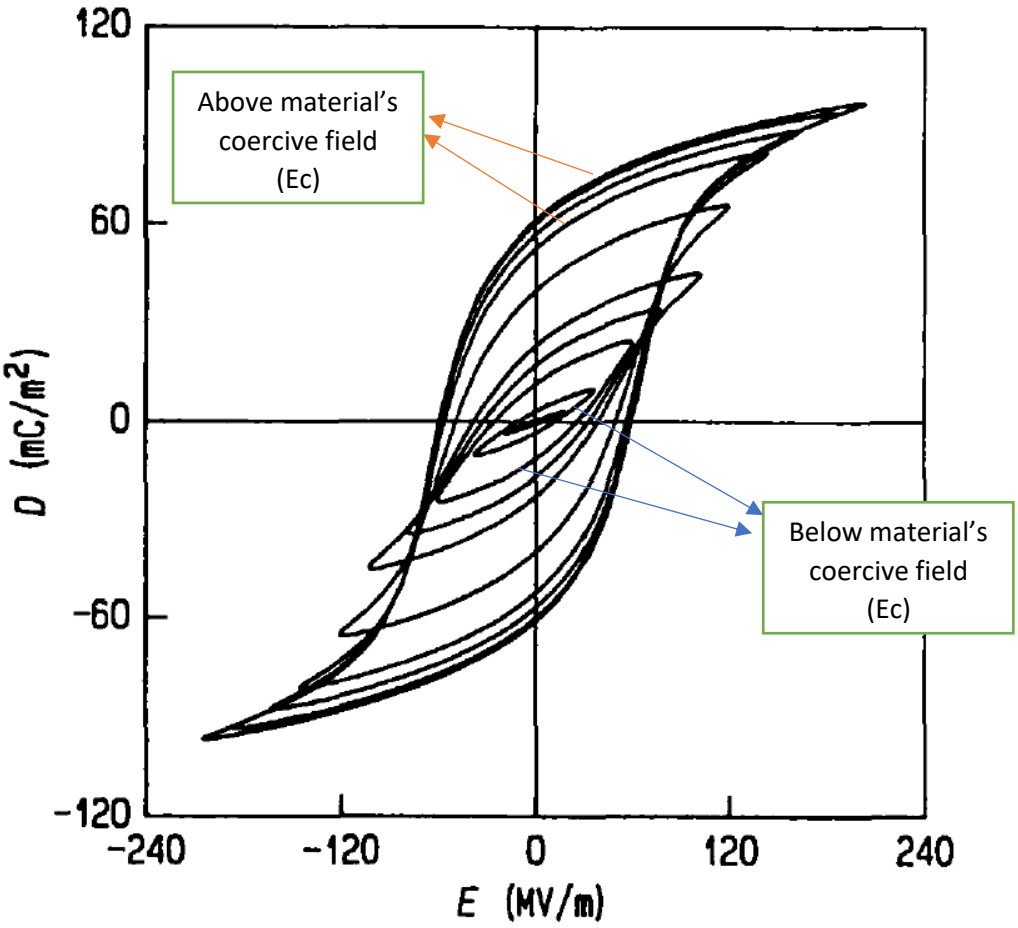

Figure 13-D-E hysteresis loops of PVDF at 20°C [8]

2.7 Nanocomposites:

Nanocomposites are materials composed of two or more phases characterized by nanoscale dimensions (nanomaterials) and are embedded in a matrix material (Figure 14). The matrix material can be metal, ceramic or polymer [13]. Nanomaterials used in nanocomposites are classified as follows [14]:

1. 0D nanomaterials have all the dimensions within the nanoscale, no dimension is larger than 100 nm. 0D nanomaterials are nanoparticles and can be crystalline or amorphous, metallic, ceramic, or polymeric.
2. 1D nanomaterials have at least one dimension within the nanoscale. 1D nanomaterials include nanotubes and nanorods. Carbon nanotubes are good example of 1D nanomaterials.
3. 2D nanomaterials have two dimensions within the nanoscale. 2D nanomaterials include nanosheets and nanofibers.
4. 3D nanomaterials have all three dimensions within the nanoscale. 3D nanomaterials include nanogranules and equiaxed nanoparticles. 3D and 0D nanomaterials can be differentiated on the base Schrödinger's equation solution, where 0D nanomaterials exhibit a quantum solution, while 3D nanomaterials exhibit a periodic solution.

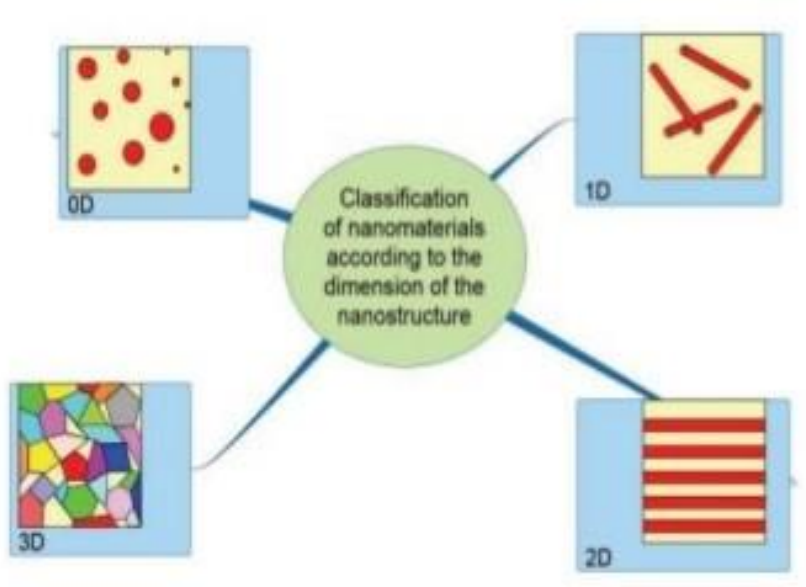

Figure 14- classification of nanocomposite materials based on dimensions of nanostructures [15]

As previously mentioned, nanocomposites are composed of two or more constituents or phases. These constituents possess different physical and chemical properties and are separated by well-defined interfaces. The constituent that is generally present in greater quantity is called the matrix. The constituent that is embedded into the matrix material is called filler material or nanomaterial. Nanocomposites differ from conventional composites due to high surface area to volume ratio of the reinforcing nanoparticles and their exceptionally high aspect ratio.

Nanocomposites can be classified based on the reinforcement material or the matrix material used. Based on the matrix material used, nanocomposites are generally classified into three classes [14]:

1. Polymer Matrix Nanocomposites
2. Ceramic Matrix Nanocomposites
3. Metal Matrix Nanocomposites

2.7.1 Polymer matrix nanocomposites:

Polymers possess beneficial properties such as lightweight (due to lightweight atoms such as carbon and hydrogen making up the vast majority of the composition and the associated low coordination number), high durability, corrosion resistance, ductility, easy synthesis and low preparation costs. However, compared to ceramics and metals, polymers have poor mechanical, thermal and electrical properties. In order to enhance the mentioned properties of polymers, the inclusion of nanoparticles with high surface area, high surface energy and often with anisotropic geometry in the polymer matrix decreases the interparticle distance and increases polymer matrix interaction strength. Therefore, polymer nanocomposites with completely new set of enhanced properties suitable for new applications arise [14].

The properties of polymer matrix nanocomposites depend on the properties of individual constituents as well as other parameters, which are:

1. Process used in nanocomposite fabrication
2. Types of filler materials and their orientations
3. Degree of mixing of two phases
4. Type of adhesion at the matrix interface
5. Volume fraction of nanoparticles
6. Nanoparticle characteristics
7. Nature of the interphase developed at the matrix interface
8. Size and shape of nanofiller material

In order to obtain enhanced nanocomposite properties, the nanoparticles should be properly and thoroughly dispersed and distributed in the matrix phase, otherwise agglomeration of particles is to be expected and associated with these agglomerations, a deterioration of the nanocomposite properties occurs. The agglomerates will act as defects and limit properties enhancement of the nanocomposite material, therefore the nanoparticles should be homogeneously dispersed in the polymer matrix.

Another contributing factor to the nanocomposite properties enhancement is the interface between the matrix phase and the filler phase. The properties, composition and microstructure at the interface are different from both the matrix and the filler. If the interface bond between the matrix and the filler material is good, then the overall properties of the nanocomposite will be greatly enhanced. The interface interactions depend on the ratio of surface energy of the filler phase and the matrix phase, where nanoparticles have high surface area, which determines the extent of interface properties contributing to the properties of the nanocomposite material [14].

2.8 P(VDF-TrFE) based sensors:

Mechanically drawn β-PVDF thin films have been used in a wide range of commercial applications [43], [44] such as motion detectors from Siemens [45], hydrophones from rp.acoustics [46], clamp-on pressure transducers for Diesel injection lines by AVL [47], contact microphones from Cold Gold [48], film speakers from fils [49], shock-wave gauges from Arkema [50], and dust sensors in space [51]. Although these examples prove the usability, durability and reliability of the drawn PVDF polymer film material, the range of applications is still limited due to constraints in film thickness, design freedom and areas and other disadvantages such as the limited thermal stability (< 70°C) of the extruded ferroelectric phase [52]. Unlike pure PVDF, the ferroelectric copolymer P(VDF-TrFE), available as a powder [53], [54], can be solution-processed and also formulated as a printable paste. Dietze [55],[36] was the first to demonstrate an all screen-printed P(VDF-TrFE) sensor array, also several other groups have shown the printability and observed the ferroelectric performance of the material [56], [57], [58], [59], [60], [25]. Moreover, P(VDF-TrFE) polymers have been developed for several applications which include organic ferroelectric non-volatile memories, which can replace inorganic ferroelectric non-volatile memories as they offer higher chemical stability as well as simpler device architecture [16]. Another interesting application of P(VDF-TrFE) would be SAW devices, which rely mainly on the copolymer's piezoelectric properties to generate surface acoustic waves [17]. Moreover, the use of P(VDF-TrFE) in piezoelectric energy harvesters is also an emerging application of such copolymers, where these PVDF-TrFE based energy harvesters utilize vibrations and mechanical pressure to be used in self powered electronics applications [18]. Pressure/temperature sensing is another major application of P(VDF-TrFE), where both the pyroelectric and as well as the piezoelectric properties are utilized [19]. Joanneum research has successfully developed such sensors under the brand name PyzoFlex, which is a printable sensor technology that can be implemented on a market-ready level (figure 15) [20].

.

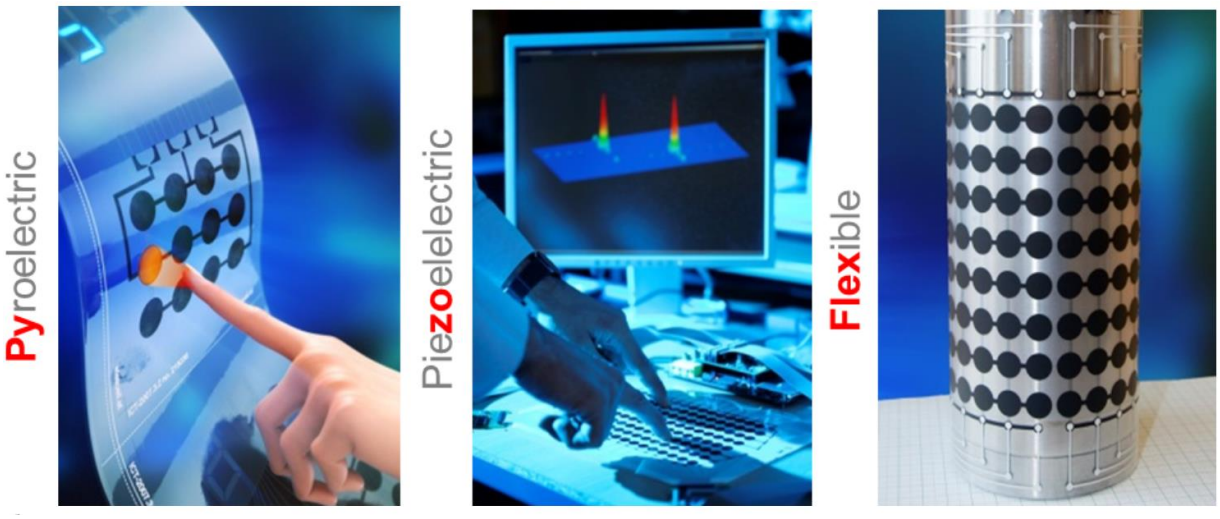

Figure 15-PyzoFlex is derived from pyroelectric, piezoelectric and flexible [20]

2.8.1 Temperature and pressure selectivity:

A drawback to using ferroelectric P(VDF-TrFE) in sensing applications is the lack of selectivity between temperature and pressure sensing, since contributions from pyroelectricity and piezoelectricity interfere, which results in thermal drifts during pressure sensing and unwanted pressure contributions due to substrate's mechanical vibrations during temperature sensing. In order to overcome the issue related to lack of selective sensing, it has been proposed to synthesis a nanocomposite material that consists of P(VDF-TrFE) as a matrix material with ferroelectric ceramic nanoparticles (Lead Titanite, PT) dispersed in it. The resultant material is composed of two phases, where each phase can be poled independently. The matrix phase has a low Curie temperature compared to the ceramic nanoparticles phase. This means that a separate poling step of the nanoparticles phase can be performed above that temperature (matrix is in paraelectric phase), while consecutive poling of the matrix phase is done at room temperature. P(VDF-TrFE) is characterized by a negative pyroelectric coefficient $-p$ and a negative piezoelectric coefficient $-d_{33}$. Moreover, the ferroelectric ceramic nanoparticles possess a negative pyroelectric coefficient $-p$ and a positive piezoelectric coefficient d_{33}. As a result, poling the matrix phase and the nanoparticles phase in an antiparallel fashion (with the equivalent compensating electric field) cancels out the pyroelectric signal and thus temperature sensing while enhancing pressure sensing. However, poling the two phases in a parallel fashion cancels out the piezoelectric signal and thus pressure sensing, while enhancing temperature sensing (figure 16) [22][23][24].

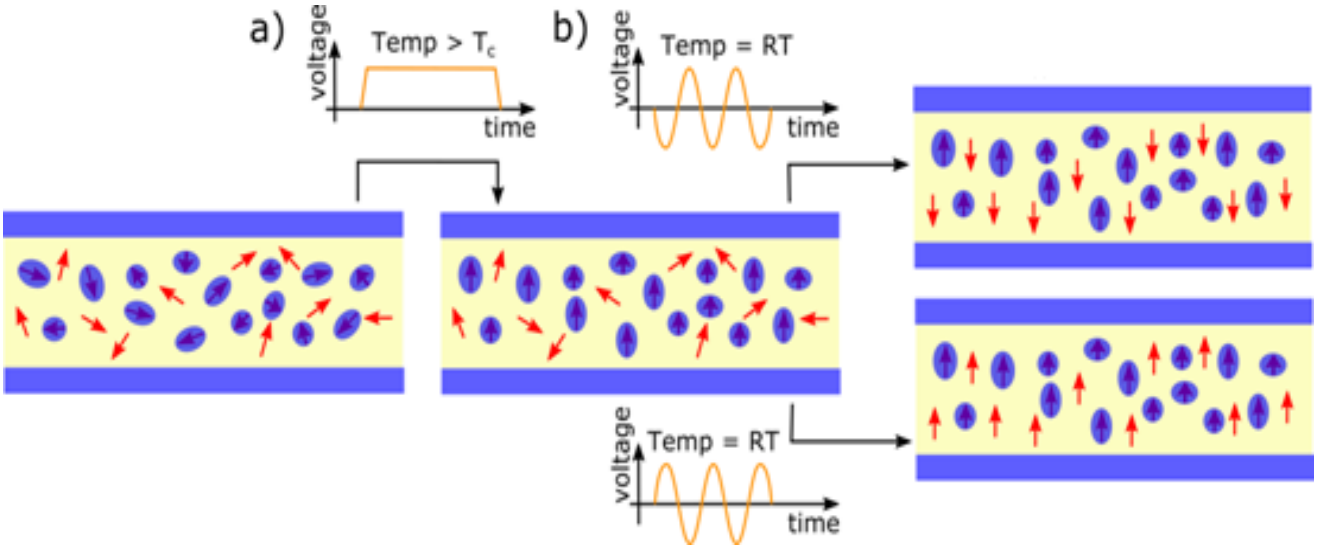

Figure 16- the nanocomposite material is composed of P(VDF-TrFE) matrix phase and ceramic nanoparticles uniformly dispersed in the matrix phase. High temperature DC poling is performed to pole the nanoparticle phase. Then AC poling at room temperature is performed on the polymer matrix phase. Parallel/antiparallel poling of matrix phase with respect to nanoparticle phase, enhances either pyroelectric or piezoelectric properties of the overall nanocomposite material

Extensive research was also carried out by Ploss and Chan on the idea. P(VDF-TrFE) with a ratio of 56/44 mol-% was used as a matrix material. The matrix material has a T_c value of 65°C, which makes it easy to depolarize by heating it above the Curie temperature, to the paraelectric phase. The matrix material was mixed with 15, 27, 34 vol-% Lead Titanate (PT) nanoparticles. The copolymer (PVDF-TrFE) was dissolved in Methylethylketone and nanoparticles were dispersed in the polymer by ultrasound excitation. After drying, the sample was prepared into 30 µm thick films by compression molding. Poling of the thick film was performed at two steps[23]:

1. At 100°C by applying a constant DC field E=55V/µm for 1hour (poling of the ceramic inclusions while maintaining the matrix polymer within the paraelectric phase).
2. Room temperature, an AC field E=80V/µm at frequency f=10Hz (poling of the matrix polymer).

Characterization was done by measuring the pyroelectric coefficient. A Peltier element was used to measure the signal. In addition to the pyro response, the piezoelectric d_{33} coefficient was also measured with a piezo tester (table 1).

	15 vol-% PT		27 vol-% PT		34 vol-% PT	
	$-p\ [\frac{\mu C}{m^2 K}]$	$d_{33}\ [\frac{pC}{N}]$	$-p\ [\frac{\mu C}{m^2 K}]$	$d_{33}\ [\frac{pC}{N}]$	$-p\ [\frac{\mu C}{m^2 K}]$	$d_{33}\ [\frac{pC}{N}]$
Only copolymer poled	24	-13	19	-9	15	-9
Copolymer and ceramic poled in parallel	30	-6	39	1	42	11
Only ceramic poled	9	4	22	12	28	18
Copolymer and ceramic poled opposite to each other	-16	17	1	20	14	21

Table 1-pyroelectric coefficient and piezoelectric coefficient measurements for different nanoparticle volume fractions and different poled states [23]

Lead-based ceramics especially $Pb(Zr,Ti)O_3$ (PZT) are widely used for piezoelectric and ferroelectric applications because of their superior properties. With concern to the environmental pollution of PbO evaporation, lead-free piezoelectric ceramics are investigated to replace the lead-based nanoparticles of the nanocomposite material. Bismuth Sodium Barium Titanite (BNBT) with chemical formula $(Bi_{0.5}Na_{0.5})_{0.94}Ba_{0.06}TiO_3$ is found to be a promising lead-free piezoelectric nanoparticles. Chan investigated a 30µm nanocomposite material, obtained by compression molding, composed of P(VDF-TrFE) 70/30 mol% copolymer matrix and BNBT nanoparticles. Samples with different volume fractions of BNBT (0.05 to 0.3) were prepared. Poling of both phases was performed by heating the sample to 80°C and applying a DC field of 50V/µm for 30 minutes at each temperature. Therefore, both phases were poled in the same direction and sensing selectivity is not investigated. A 2nd poling procedure is performed at 120°C to pole the BNBT nanoparticle phase, while copolymer matrix was poled at 25°C, again both phases were poled in parallel directions. The pyroelectric piezoelectric and dielectric properties were measured for a sample composed of of P(VDF-TrFE) 70/30 mol% copolymer matrix and BNBT nanoparticles added at 30 vol-% (table 2) [38].

	ε	d_{33} pC/N	p μC/Km2
Bot phases poled at 80°C	20.7	-14	47.3
Nanoparticles poled at 120°C, polymer at 25°C	28.6	-21	22.1

Table 2-dielectric,piezoelectric and pyroelectric properties of P(VDF-TrFE) 70/30 mol% copolymer matrix and BNBT nanoparticles added at 30 vol-% [38]

3. Sample preparation

3.1 Screen-printing technique:

Screen printing technique has evolved as a cheap, efficient, reliable and reproducible printing technique for electronics. The technique involves printing inks into desired patterns by using a screen with specific mesh design, to transfer a specific pattern onto a substrate, as can be seen in figure 17 below [26].

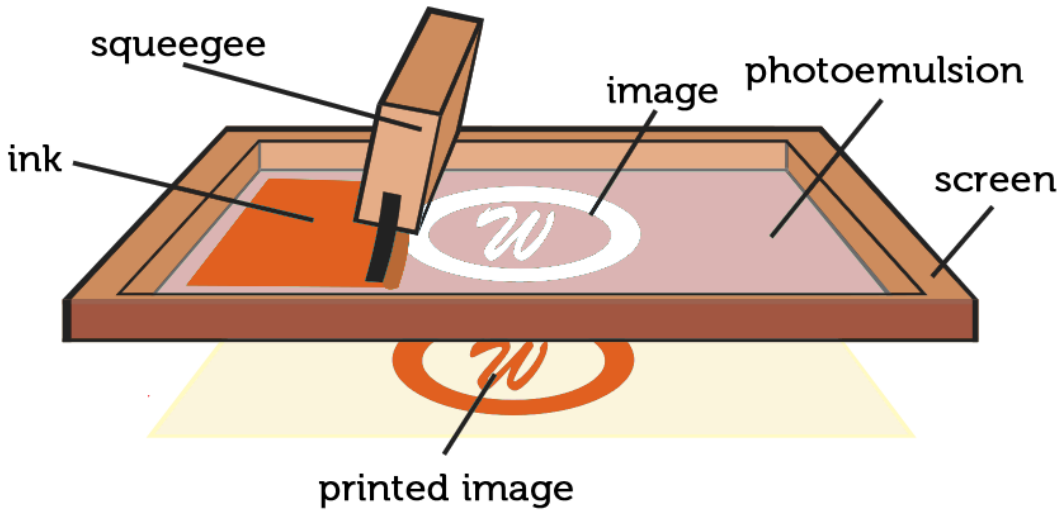

Figure 17-general concept of printing electronics using screen printing technique [29]

As an initial step, the ink is poured or spread over to "flood" the screen, which has a specific mesh pattern. Spreading of the ink on the screen surface is done by the squeegee's forward motion. In the following step, the squeegee's backward motion pushes the ink through the mesh pattern onto the substrate.

Commercially, screen printing is classified into two main setups [27]:

1. flatbed screen printing setup
2. Rotary screen printing setup

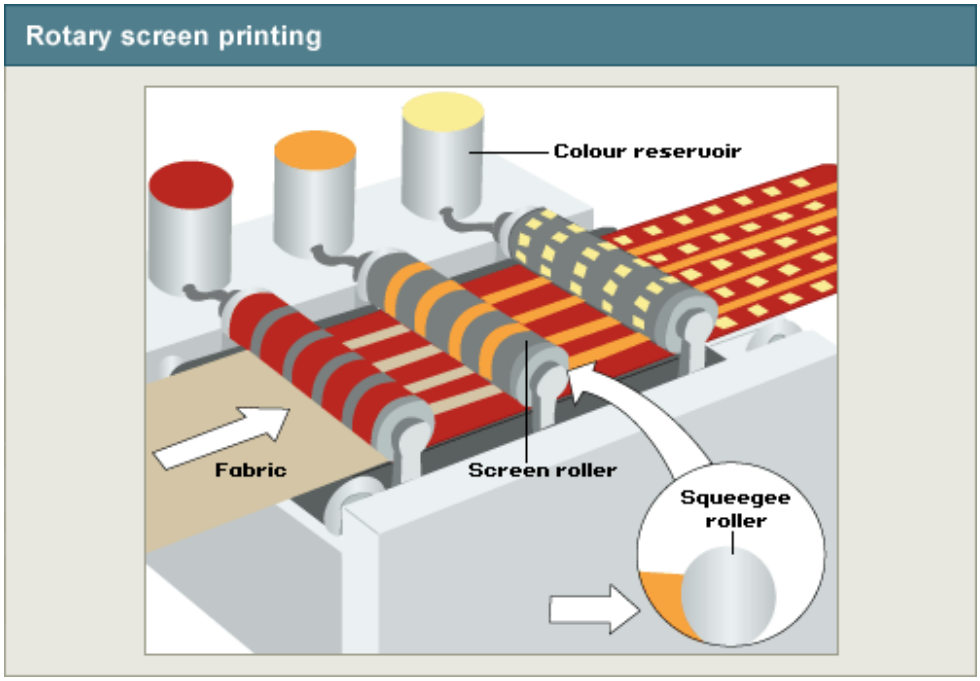

Figure 18-Rotary screen printing process [30]

Rotary screen printing (figure 18), is an automated process, where the ink is continuously fed to the squeegee roller to achieve a fast printing rate. For this setup, the printable pattern is integrated into the squeegee, eliminating the need for a separate screen. This is in contrast to flatbed screen printing, which relies on manual feeding of the ink and is a slower process (figure 19). Moreover, flatbed processes maintains a screen which is separate from the squeegee [26][27][28].

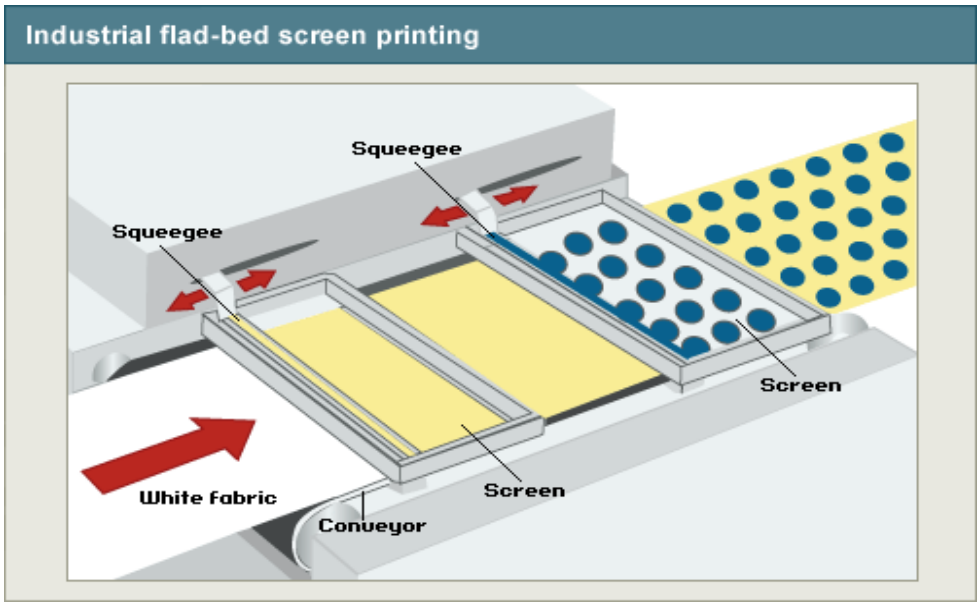

Figure 19-flat-bed screen printing process [30]

The quality and the thickness of printed films depend on several factors, such as [27][28]:

1.Squeegee pressure and speed

2. Mesh size and geometry

3. Distance between screen and substrate

4. Material viscosity

At Joanneum Research, Flatbed screen printing technique is utilized to print the nanocomposite sensors. The screen printer has a commercial name of Thieme Lab 1000 and offers a printing area of 400x400 mm. Substrates with thickness *t* below 20 mm can be used. Moreover, a maximum squeegee speed of 500 mm/s can be achieved.

3.2 Inks and resultant materials:

Inks are printed onto a flexible Polyethylene terephthalate (PET) substrate provided by Dupont Teijen Films. The A4 sized substrate is 175 µm thick and is sold under the commercial name Melinex STS 505. Melinex STS 505 substrates offer dimensional stability at temperatures up to 150°C. Moreover, it is surface treated to provide better adhesion of printed inks. General properties of the substrate are provided in table 3:

Property	Value
Melting point (Tm)	255°C
Dielectric constant	2.9
Surface resistivity	10^{13}
Volume resistivity	10^{15}

Table 3- properties of Melinex STS 505 substrate [31]

The first layer to be printed is the bottom electrode, which is composed of PEDOT:PSS. The ink is provided by Heraues Deutschland GmbH & Co. KG. Related viscosity and sheer resistance values are provided in table 4 below:

Property	Value
Viscosity	15 to 60 Pa.s
Sheet Resistance	500 Ohm/sq

Table 4-properties of PEDOT:PSS ink [32]

After screen printing the bottom electrode. A curing step is applied, this is done by placing the sample in an oven (Memmert UF-110 or UF-160) for 45 minutes at 100°C. This curing step will allow evaporation of the solvent and results in drying and solidification of the printed layer.

After curing the printed bottom electrode layer, the ferroelectric nanocomposite layer is printed. Inks of two ferroelectric nanocomposites were used to produce two different samples. The first ferroelectric nanocomposite material is composed of P(VDF-TrFE) 70:30 mol-% as matrix material, with Lead Titanite ($PbTiO_3$) 20 vol-% nanoparticles as filler material. Lead free nanoparticles were also provided to produce an environmental-friendly nanocomposite material, which is composed of P(VDF-TrFE) 70:30 mol-% as matrix material and Bismuth Sodium Titanite ($BiNaTiO_3$) 20 vol-% nanoparticles as filler material. Both nanocomposite materials were provided by Fraunhofer Institute for Silicate Research. The viscosity of the nanocomposite material is controlled by the solvent content (γ-Butyrolactone), which is added at 88 vol-% . However, no viscosity values are provided for both materials.

After curing the nanocomposite printed layer, printing of the top electrode is done. The same PEDOT:PSS ink is used for the top electrode as for the bottom electrode. Electrical contact lines composed of silver ink with a commercial name of Dupont PE828 were printed as a final step. The silver electrical contacts were cured for 10 minutes.

The Dupont PE828 Silver ink has the following viscosity and sheet resistance values:

Property	Value
Viscosity	15 to 50 Pa.s
Sheet resistance	25 Ohm/sq

Table 5-properties of Dupont PE828 Silver ink [33]

As mentioned previously in this chapter, mesh design, squeegee pressure and speed as well as the distance between the screen and the substrate, are important parameters to control the quality and the thickness of the printed layers. Bottom and top electrodes are printed using a steel mesh 90-40 SD, while the ferroelectric sensing layer is printed using a polyester mesh 24-150 y and the contact lines using a steel mesh 56-32 SD. The printing parameters for each layer are as follows:

	Bottom electrode	Ferroelectric nanocomposite	Top electrode	Electrical contact lines
Squeegee pressure	4 bar	2.5 bar	4 bar	4 bar
Squeegee speed	150 mm/s	50 mm/s	150 mm/s	100 mm/s
Screen-substrate distance	4 mm	4 mm	4 mm	3 mm

Table 6-printing parameters of each layer

And the resultant device architecture is as follows:

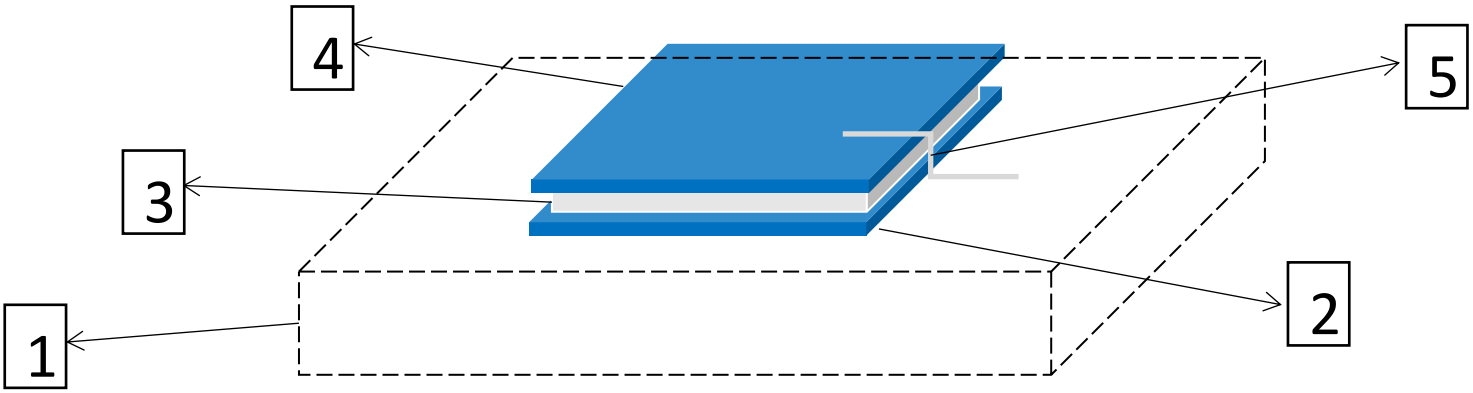

Figure 20- double plate capacitor architecture is prepared using screen printing technique

The resultant printed sensors pattern on the A4 sized substrate is as follows:

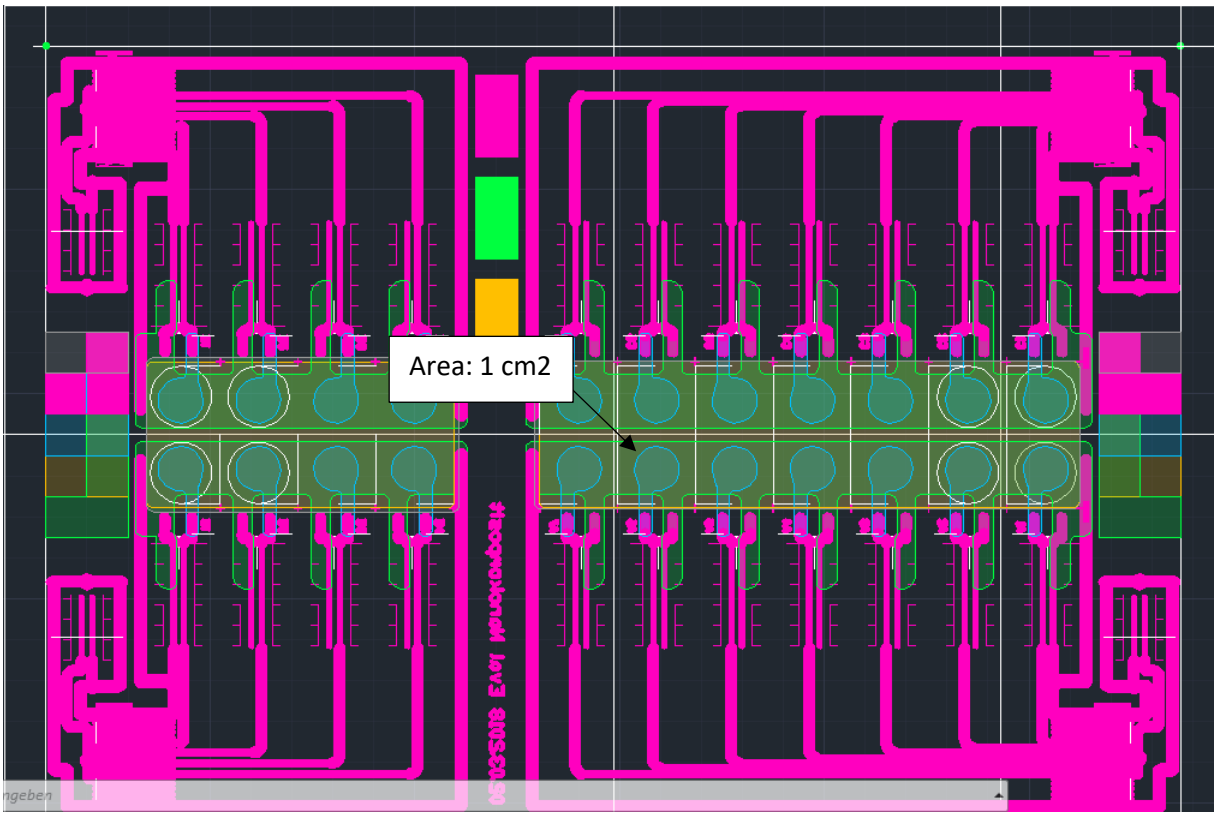

Figure 21-the printed sensor pattern on an A4 Melinex STS 505 substrate

Finally, the two nanocomposite materials are given in table 7 and figure 22:

	Matrix phase	Nanoparticles phase
Nanocomposite material 1	P(VDF-TrFE) 70-30 mol-%	$PbTiO_3$ 20 vol-%
Nanocomposite material 2	P(VDF-TrFE) 70-30 mol-%	$BiNaTiO_3$ 20 vol-%

Table 7-description of two screen printed nanocomposites

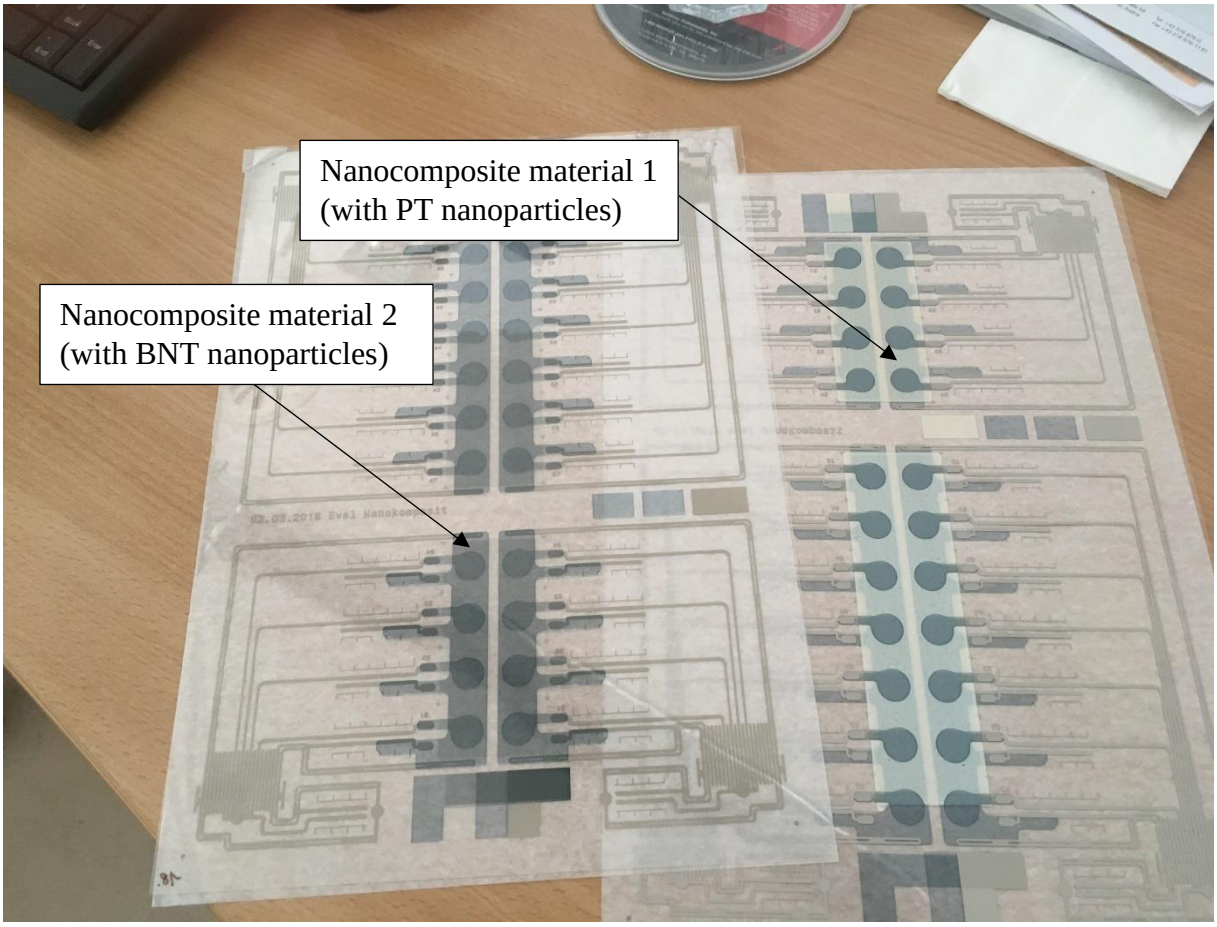

Figure 22-resultant printed A4 sheets for nanocomposite material 1 and 2

3.2 SEM Characterization:

After successful preparation of nanocomposite materials 1 and 2 using screen printing technique. Characterization of the samples is done using a scanning electron microscope (SEM). Cross-sectional cuts are prepared using a microtome (Cryo-Ultramicrotome PT-X2/CX2) and are imaged using a JSM-IT100(JEOL)-LV/LA electron microscope. This step allows estimating the thickness *t* of the screen printed layers as well as observing the nanoparticles dispersion in the copolymer.

Figure 23 below shows an SEM image for nanocomposite material 1, which is P(VDF-TrFE)-PT. The nanoparticles are well dispersed in the matrix phase. However, nanocomposite material 2 shows less particle density and dispersion, which might influence the results to be discussed later in this thesis (figure 24).

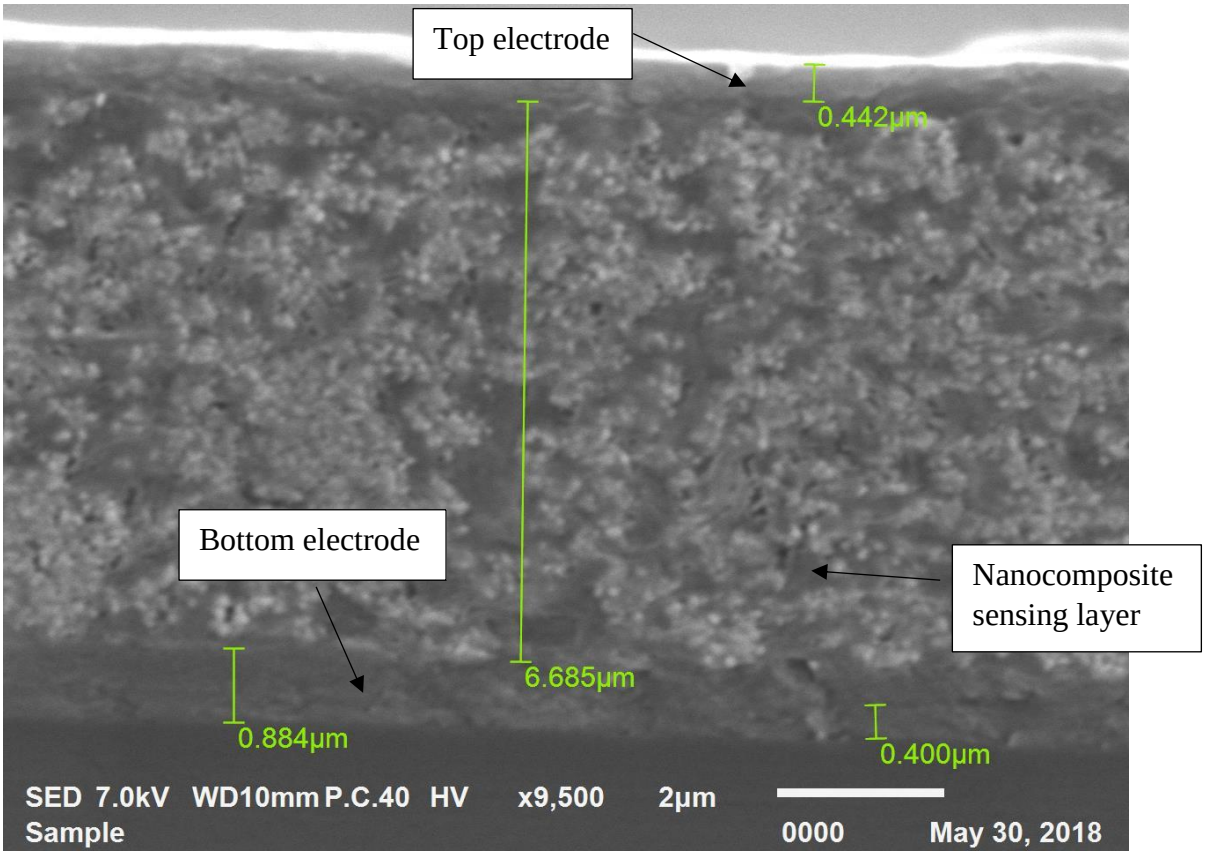

Figure 23- SEM cross sectional image of nanocomposite material 1, which shows fine dispersion of nanoparticles in matrix phase

Moreover, thickness variations exist between nanocomposite material 1 and 2. The nanocomposite layer of nanocomposite material 1 has a thickness of 6.7 µm while sample 2 has a nanocomposite layer thickness of 7.7 µm. Thickness variations between bottom and top electrode of the same sample are observed, as well as between the two samples.

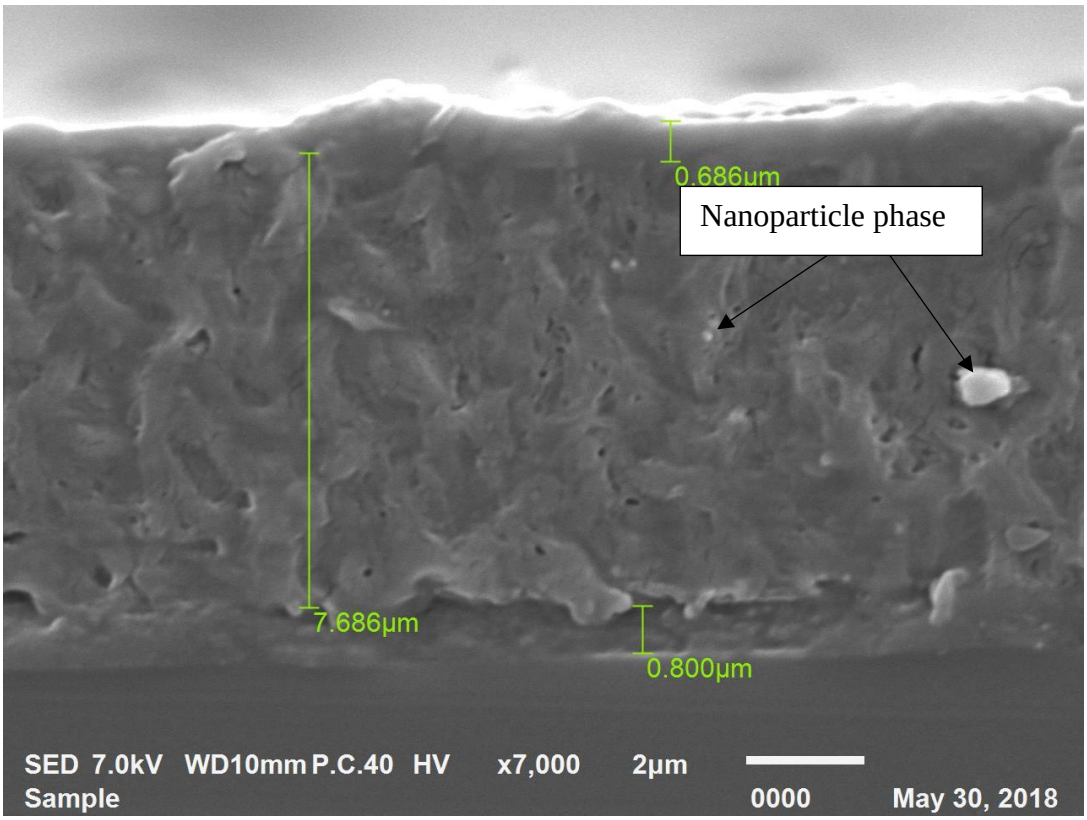

Figure 24-SEM cross sectional image of nanocomposite material 2, which shows low concentration of nanoparticles as compared to nanocomposite material 1

4. Measurement Setup

4.1 Poling setup:

Poling is a process in which high electric field is applied to a ferroelectric material in order to orient its electric dipole moments (figure 25). The process enhances the material's piezoelectric, pyroelectric and ferroelectric properties.

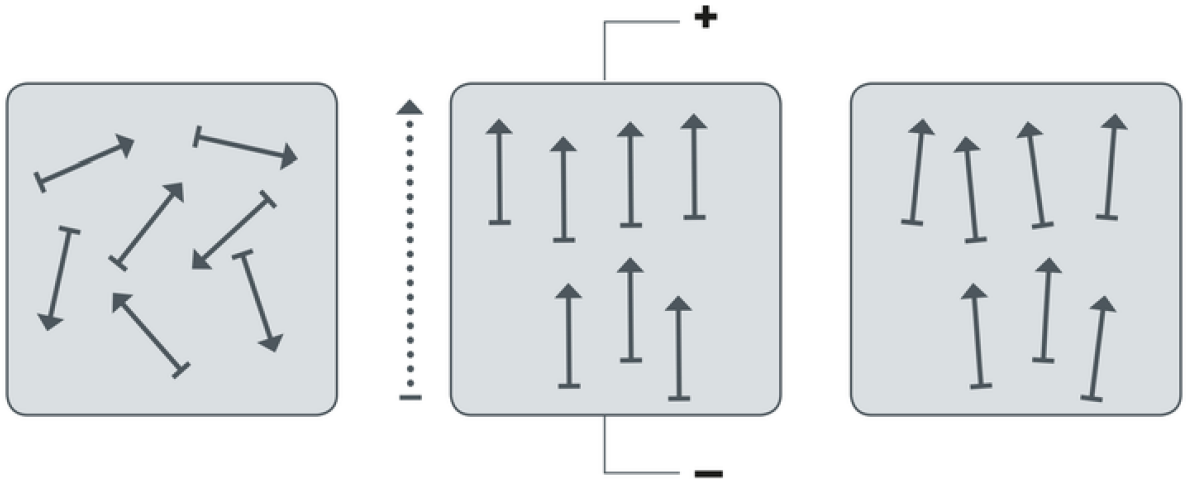

Figure 25-influence of poling on ferroelectric dipole moments/domains [34]

Initially the electric dipoles are arranged in domains randomly oriented inside the ferroelectric material. This amounts to zero net macroscopic polarization. By applying an external electric field above the material's coercive field, the domains orient themselves in the field's direction. This amounts to the ferroelectric spontaneous polarization. Removal of the external electric field will allow the domains to relax into equilibrium position, which amounts to the material's remnant polarization.

Poling of screen printed nanocomposite material 1 and sample 2 is performed in a poling stage (figure 26). The poling stage is equipped to perform room temperature poling as well as high temperature poling. High temperature poling is performed on a heat plate (IKA C-MAG HS7), which can heat up to a maximum surface temperature of 500°C. The sample is contacted to a high voltage source (Matsusada AMT-10B10), which supplies maximum output voltage of 10kV and an output current of 10mA (figure 27). Current generated by the sample during poling is measured and integrated with respect to time to obtain the charge. Moreover, ferroelectric *D-E* loops are generated for matrix phase using a DIAdem code (check appendix for complete code). However, *D-E* loops can only be generated if AC poling is performed (field reversal results in polarization reversal and ferroelectric hysteresis is therefore observed).

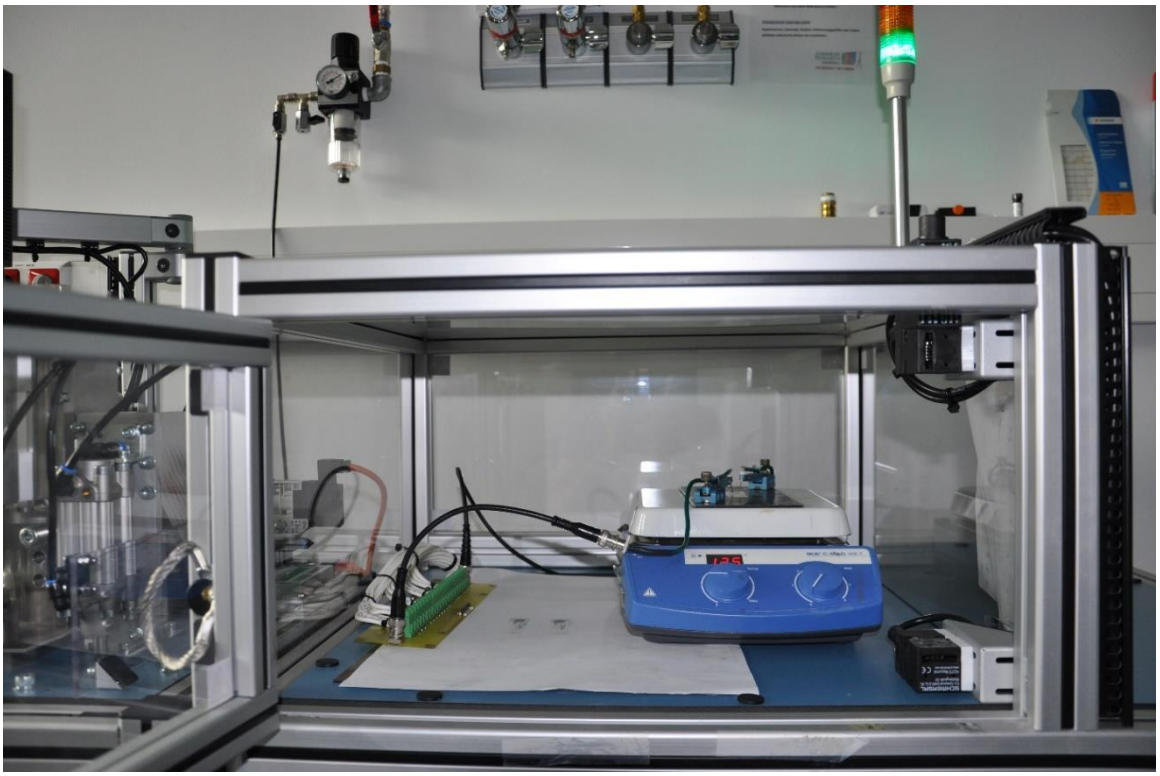

Figure 26- poling stage where room temperature and high temperature poling can be performed

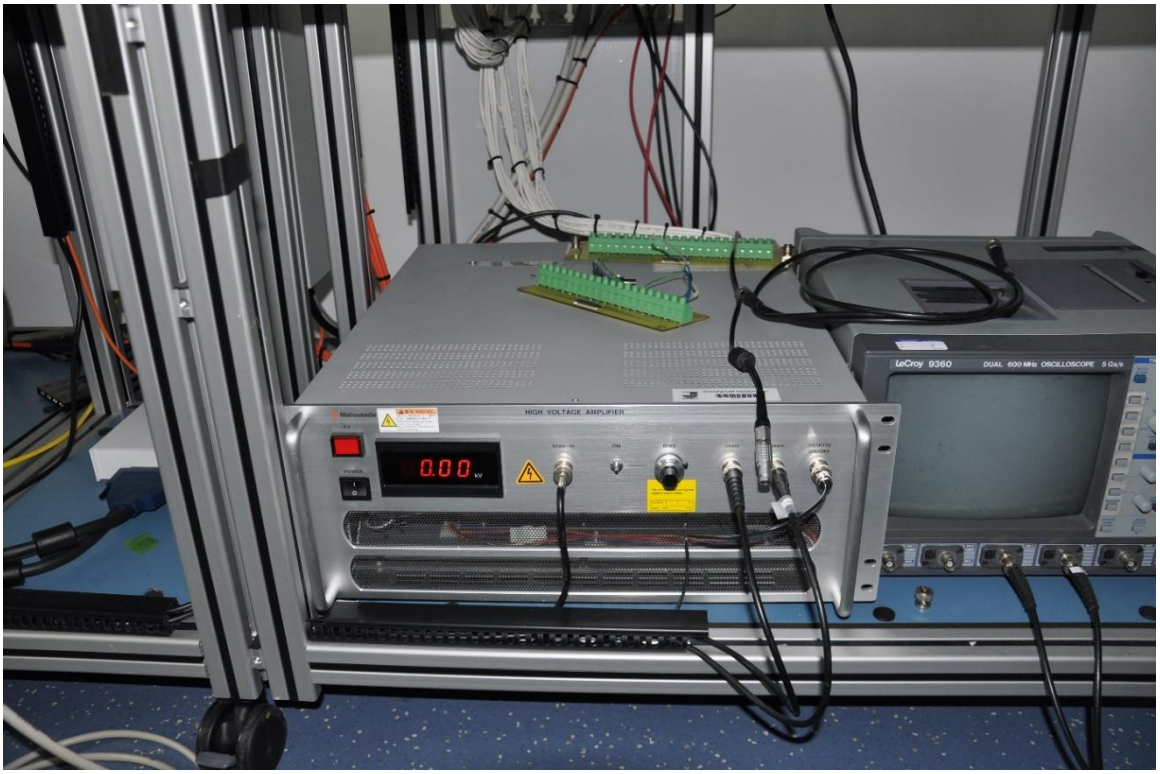

Figure 27- Matsusada AMT-10B10 High voltage source

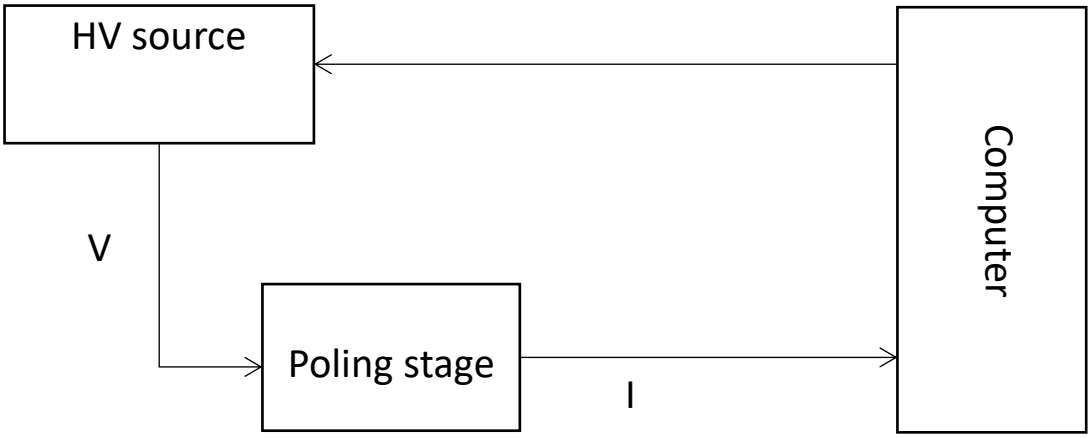

Figure 28- schematic diagram of poling setup

4.1.1Poling of nanoparticle phase:

Poling of the nanoparticle phase requires substantial charge flow from the electrode through the matrix into the nanoparticles [22]. This charge flow process is a function of time. Therefore, a constant DC field with relatively long poling time should fulfil the conditions needed to pole this phase, assuming that the DC field is high enough. If this poling step is performed at room temperature, then the matrix phase would be poled as well as the nanoparticle phase. In order to avoid this, the sample is heated to 125°C. The nanoparticle phase has a much higher Curie temperature in comparison to the matrix phase. Therefore, heating the sample to 125°C means that the matrix material has transitioned into its paraelectric phase and cannot be poled. However, the nanoparticles are still in their ferroelectric phase and can be poled. By employing this mechanism, selective poling of the two phases can be achieved.

4.1.2 Poling of matrix phase:

In this step, the sample is cooled down to room temperature and AC poling is performed. High poling fields of 2 to 3 times the coercive field , which is 50V/µm for P(VDF-TrFE) 70:30 mol% would be sufficient to fully pole the matrix phase. Since poling of the P(VDF-TrFE) matrix phase does not require long poling time, AC poling at 10Hz is performed. Since AC poling at 10Hz is a fast process, then the polarization state of the nanoparticles phase should remain unaffected. By stopping this procedure after the positive or negative half-wave the orientation of the spontaneous polarization can be defined. (compare **Error! Reference source not found.**).

4.2 Pyroelectric measurement setup:

In order to measure the pyroelectric coefficient, the sample is placed into a Linkam temperature controlled stage (figure 30). The LTS350 stage is connected to a TMS94 temperature controller and a LNP95 liquid nitrogen pump. The complete setup is supplied by Linkam Scientific Instruments. A Keithley electrometer (model 6517A) is used to measure the charge generated by the sample during a heating cycle, figure 29 shows the components needed to measure the pyroelectric coefficient. Samples are heated from 25°C to 40°C and the generated charge is recorded. Polarization can be obtained from measured charge by accounting for the sensor's surface area. By plotting the polarization as a function of the temperature and calculating the slope of the curve, the pyroelectric coefficient p is obtained.

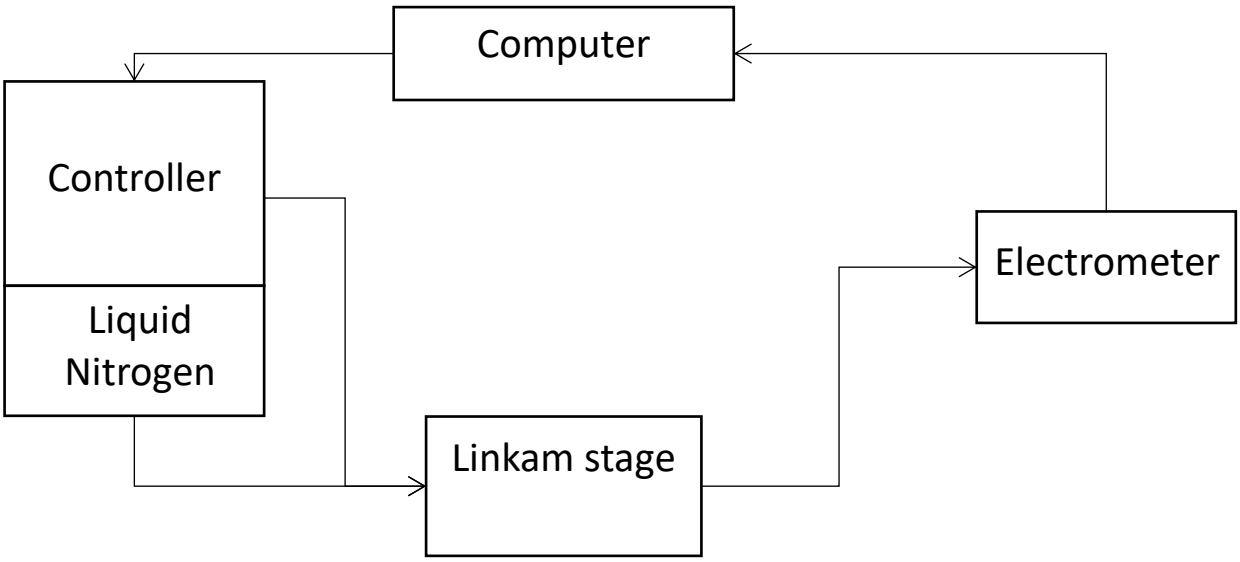

Figure 29-schematic diagram of pyroelectric measurement setup

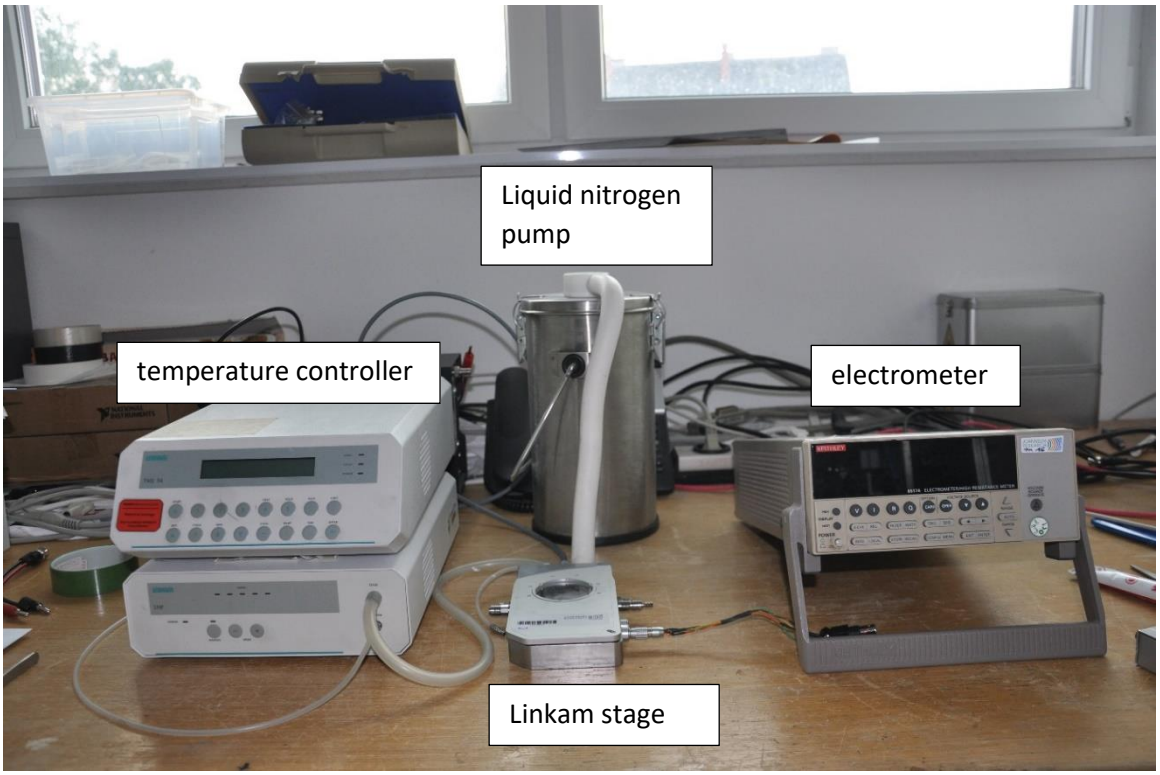

Figure 30-Linkam temperature controlled stage

4.3 Piezoelectric measurement setup:

Measurement of the piezoelectric coefficient is performed by placing the sample under a heavy stamp. The stamp uses pneumatic valves to supply a force range of 0 to 2000N (figure 32). The sample is connected to an amplifier, which amplifies the current generated which in turn is recorded by the function analyzer (DEWESoft Sirius). A schematic diagram representing the main components is shown in figure 31. Using a MATLAB code, polarization is calculated and plotted as a function of the applied force and the slope of the curve is the resultant piezoelectric coefficient d_{33}. The MATLAB code is added to the appendix section of this thesis.

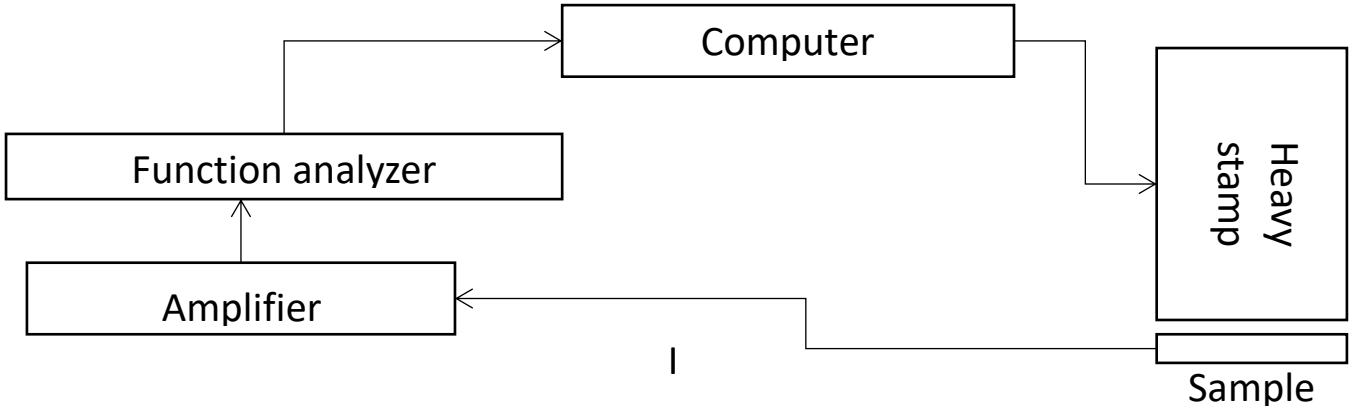

Figure 31-schematic diagram of piezoelectric measurement setup

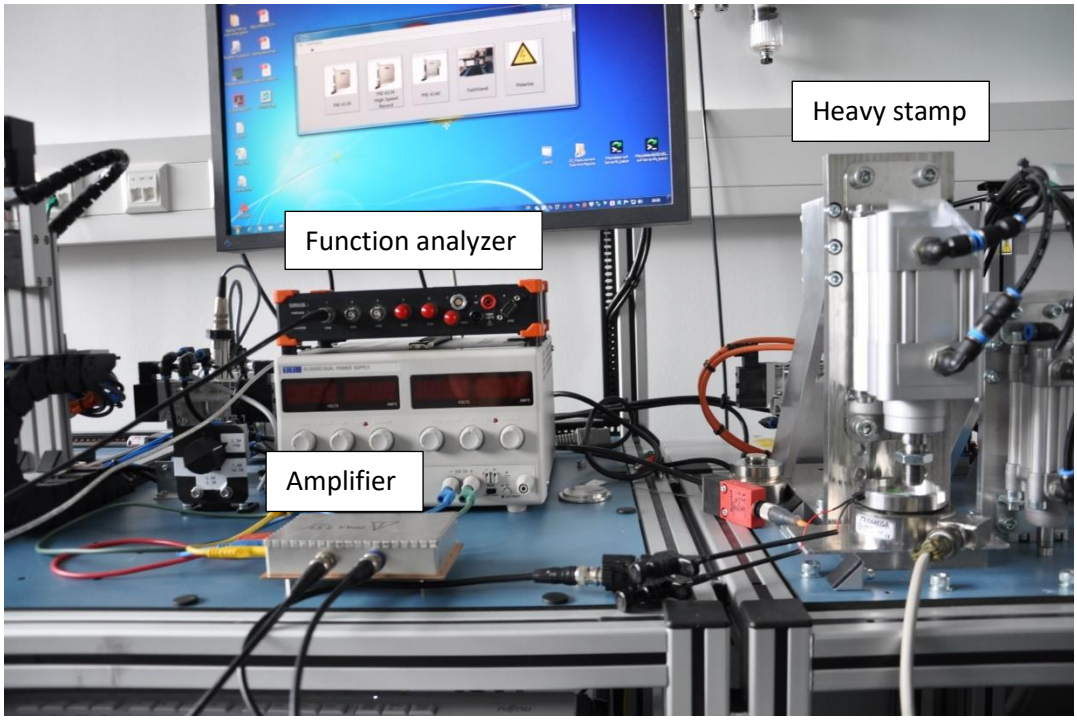

Figure 32-Main equipment used for piezoelectric coefficient measurement (Heavy stamp, amplifier and function analyzer

4.4 Capacitive measurement setup:

Using an LCR meter (Hioki 3532-50 LCR HiTESTER), the sample's capacitance is measured with respect to temperature at a frequency of 1kHz. The sample was heated from room temperature to 140°C and then cooled down again to room temperature. This can be used to monitor the ferroelectric-paraelectric phase transition upon heating as well as the paraelectric-ferroelectric phase transition upon cooling. From the measured capacitance, the dielectric constant is calculated and its behavior with respect to temperature is observed.

5. Results and discussion

5.1 P(VDF-TrFE)-Lead Titanite nanocomposite:

5.1.1 Poling of nanoparticle phase:

As discussed in previous chapters of this thesis, the idea of selective temperature or pressure sensing is achieved by a nanocomposite material. This can be realized by Independent poling of each of the two constituents forming the nanocomposite material. Poling of nanoparticle phase is performed first. This step requires heating the sample above the polymer's Curie temperature while applying a constant DC electric field for a defined duration of time.

DC poling of the nanoparticle phase is characterized by the poling field and time. In order to investigate the influence of those two parameters on the obtained nanoparticle poling, the sample was poled at 50 V/µm for 150 s, 50 V/µm for 300 s, 60 V/µm for 150 s and 60 V/µm for 300 s. After each poling step, the pyroelectric coefficient was measured using the setup discussed in chapter 3 (figure 33).

For an unpoled state, the pyroelectric coefficient is 0.7 µC/Km^2. After poling the sample at 50 V/µm for 150 s, the measured pyroelectric signal is 7.8 µC/Km^2. Increasing the poling time to 300s increased the measured pyroelectric signal to 8.3µC/Km^2. At a poling field of 60 V/µm and poling time of 150 s, the measured pyroelectric coefficient increased to 11 µC/Km^2. Increasing the poling time to 300 s while maintaining the poling field at 60 V/µm, yielded a signal of 11.9 µC/Km^2. These results indicate a higher influence of the poling field on the measured pyroelectric signal, of the nanoparticle phase, than the poling time. Moreover, poling the nanoparticle phase was unsuccessful when a poling field below the polymer's coercive field was applied (E_c =50 V/µm).

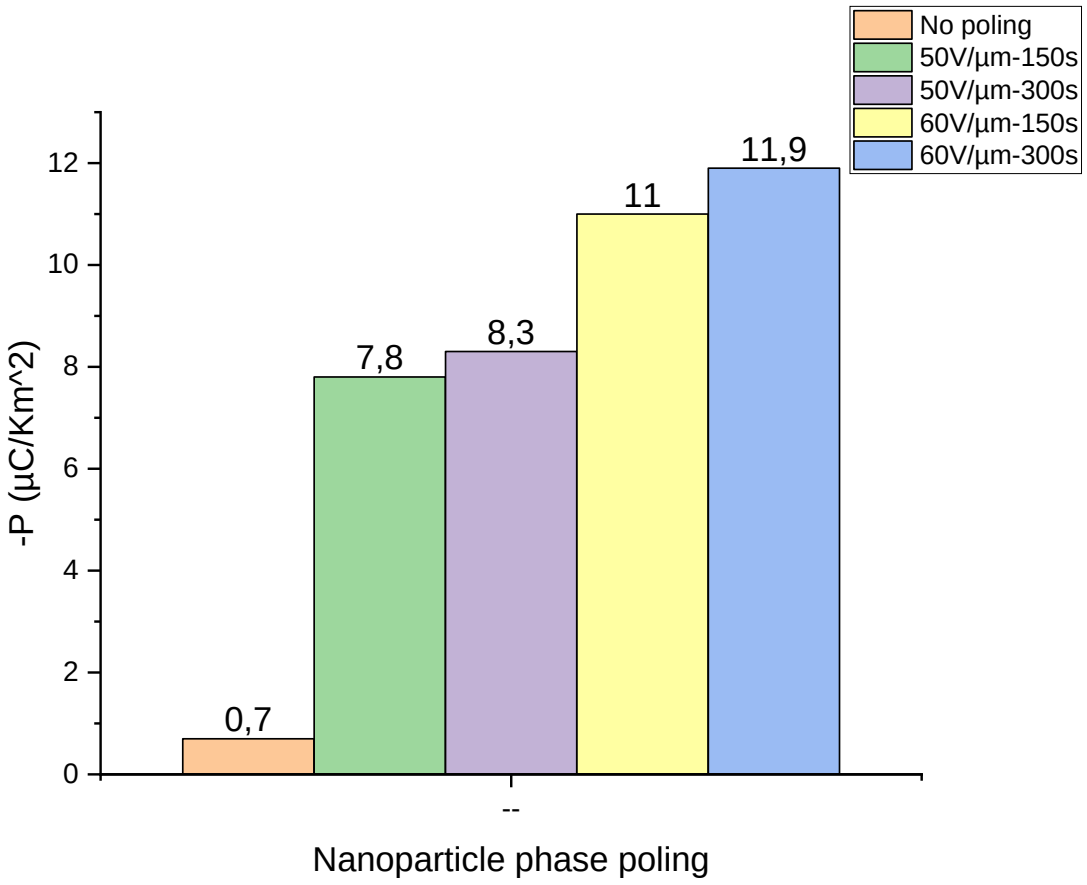

Figure 33- Lead Titanite nanoparticle phase poling investigated for different poling fields and poling times

5.1.2 Poling of polymer matrix phase:

Poling of the matrix phase is performed after cooling the sample to room temperature. Since AC poling is performed, *D-E* hysteresis loop for the polymer matrix phase is obtained (figure 34).

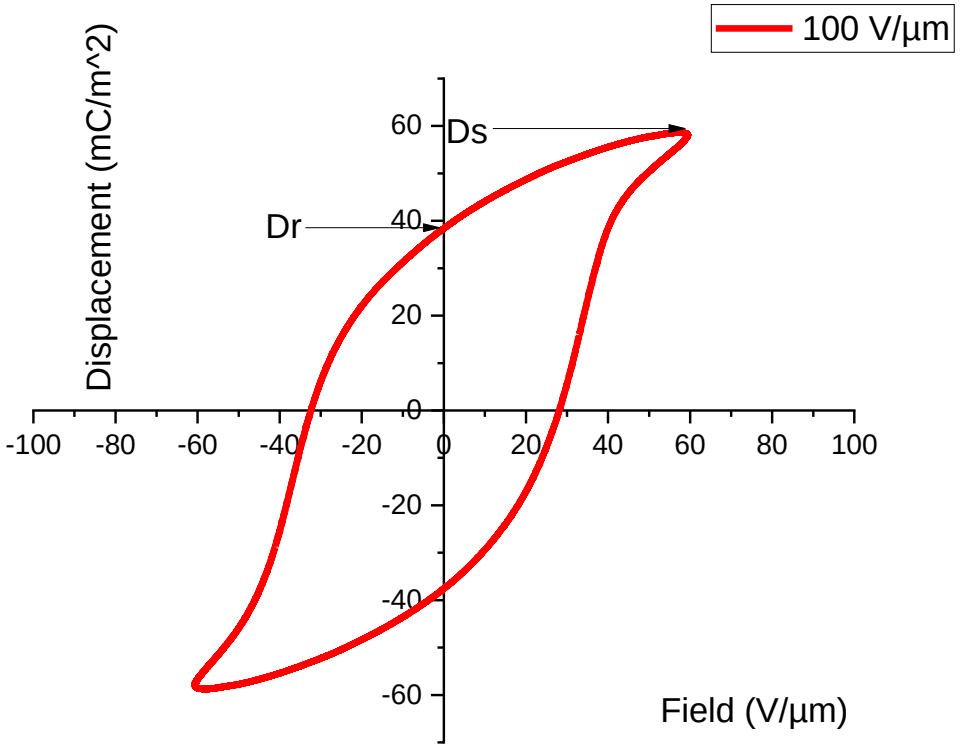

Figure 34-D-E hysteresis obtained for P(VDF-TrFE) matrix phase from AC poling

At an AC poling field of 100 V/µm, the P(VDF-TrFE) polymer has a spontaneous displacement of 58 mC/m^2 and a remnant displacement is 38 mC/m^2. Moreover, It can be observed that the coercive field is around 30 V/µm, which means the dispersed nanoparticles have reduced the polymer's coercive field. Asymmetry of -E_c and +E_c (intersection points of the loop with the x-axis) is attributed to structural and electronic asymmetry of the ferroelectric-electrode interface, asymmetric surface fields and space charge regions [35].

5.1.3 Pyroelectric signal cancellation:

Sensing selectivity depends on the poling direction (parallel poling of both phases verses antiparallel poling of both phases) as well as the matrix phase poling field magnitude. Both constituents possess a negative pyroelectric coefficient. This means that antiparallel poling of both phases eliminates the pyroelectric effect and thus temperature sensitivity (figure 35).

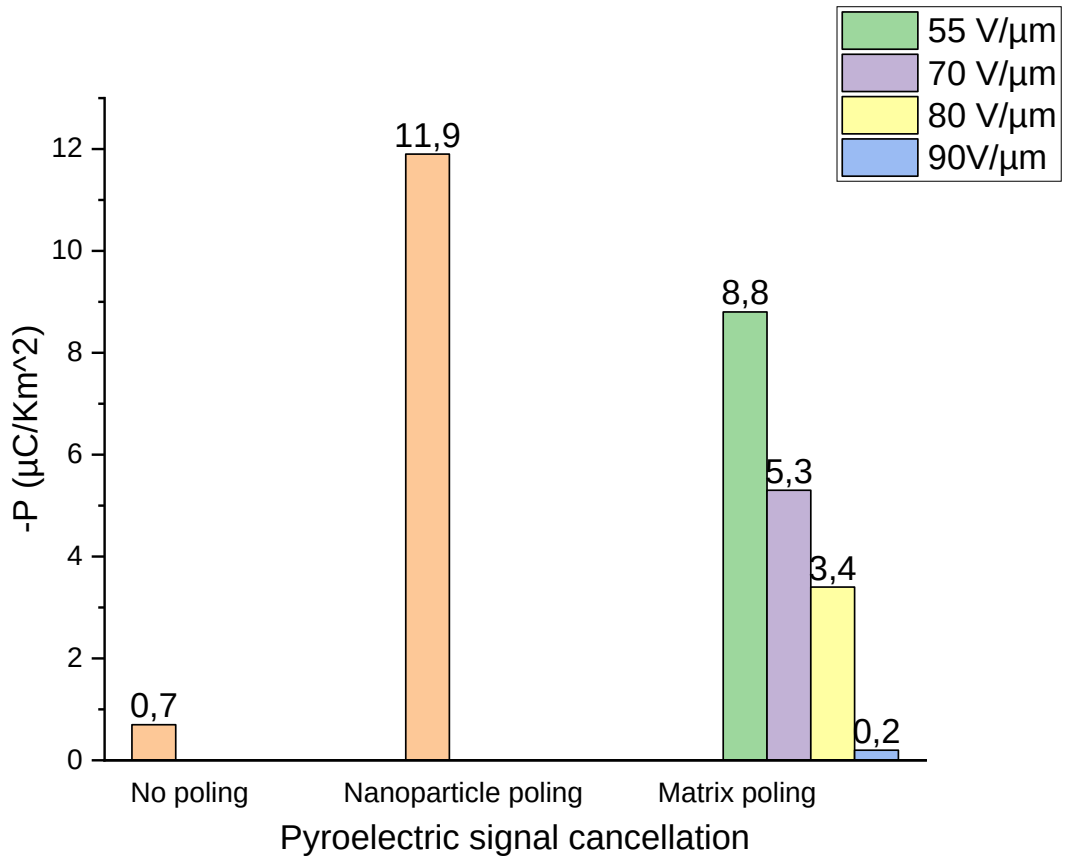

Figure 35-pyroelectric signal cancellation is done by poling the PT nanoparticle phase and then poling the matrix opposite in direction (reversing polarization direction)

The pyroelectric coefficient for an unpoled state is measured at 0.7 µC/Km^2. The maximum obtained pyroelectric coefficient is 11.9 µC/Km^2. Antiparallel poling of the matrix phase is then performed. In each matrix poling step, the poling field is increased and the pyroelectric coefficient is recorded to see at which matrix poling field will the signal be compensated. Starting with 55V/µm, the pyroelectric coefficient is measured at 8.8 µC/Km^2. At 70 V/µm, the coefficient is measured at 5.3 µC/Km^2. Further increase of the matrix poling field to 80 V/µm results in a measured pyroelectric coefficient of 3.4 µC/Km^2. Finally, at 90 V/µm, the pyroelectric signal is reduced to 0.2 µC/Km^2.

5.1.4 Piezoelectric signal cancellation:

In order to eliminate the piezoelectric signal and thus pressure sensing. Parallel poling of the nanocomposite's phases is performed. The polymer is characterized by a negative piezoelectric coefficient -d_{33}, while the lead titanite nanoparticles have a positive piezoelectric coefficient. Therefore, parallel poling of both phases with the equivalent matrix poling field magnitude should eliminate the piezoelectric contributions (figure 36).

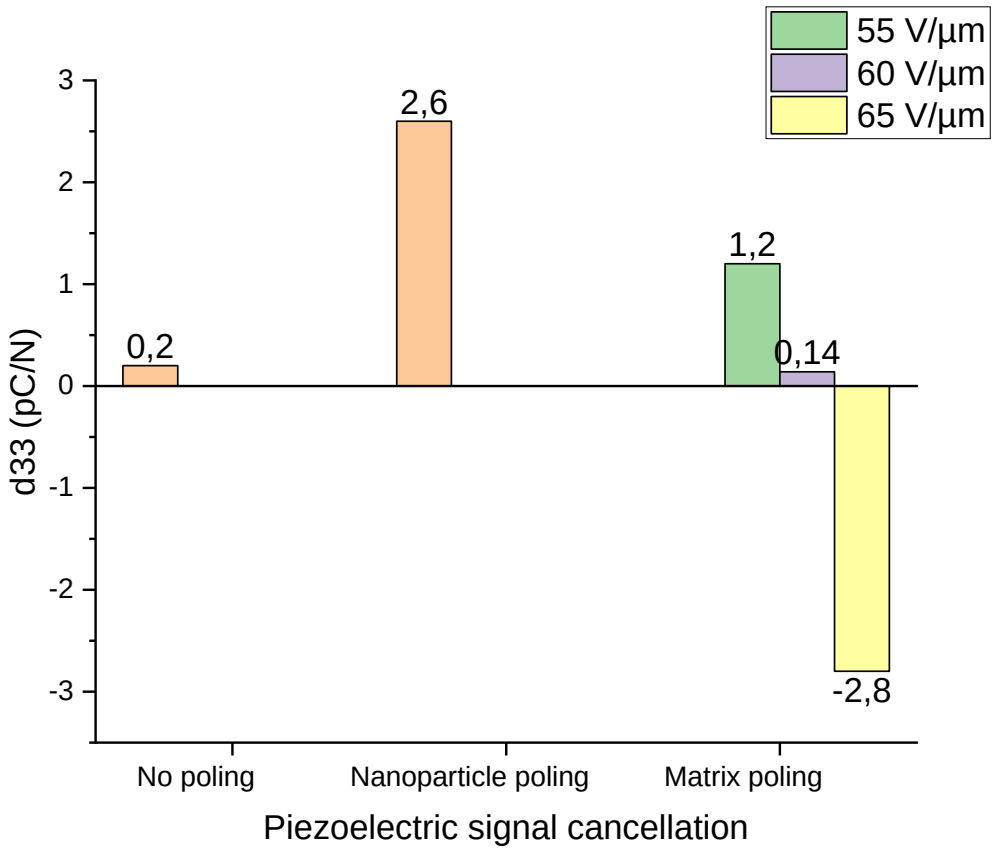

Figure 36-piezooelectric signal cancellation is done by poling the PT nanoparticle phase and then poling the matrix in the same direction

For an unpoled state, the measured d_{33} coefficient is 0.2 pC/N. From poling the nanoparticle phase, the measured d_{33} coefficient is 2.6 pC/N. The piezoelectric coefficient d_{33} drops to 1.2 pC/N when matrix poling was performed at 55V/µm. further increase of the matrix poling field to 60V/mm results in a measured d_{33} signal of 0.14 pC/N. At 60 V/µm, the d_{33} coefficient is measured at -2.8 pC/N, with the negative sign indicating a signal obtained from the copolymer matrix phase overcompensating the signal from the nanoparticles phase.

5.1.5 Ferroelectric-paraelectric phase transition:

Observing the ferroelectric to paraelectric phase transition and vice versa is obtained from measuring the capacitance as a function of a temperature program. From the measured capacitance, the effective dielectric constant is obtained (figure 37). The dielectric constant increases as the temperature increases. Exponential increase of the dielectric constant is obtained close to the Curie temperature. Crossing the Curie temperature translates to the material transition to the paraelectric phase, where a drop in the dielectric constant is seen. The Curie temperature of the matrix phase for a heating cycle occurs at 107°C. The temperature range does not include the nanoparticle's Curie temperature. Cooling the sample back to room temperature, results in paraelectric to ferroelectric phase transition, which occurs at lower temperature (75°C). The dielectric constant measured at 1 kHz at room temperature is 20. It increases up to 70 close to the Curie temperature.

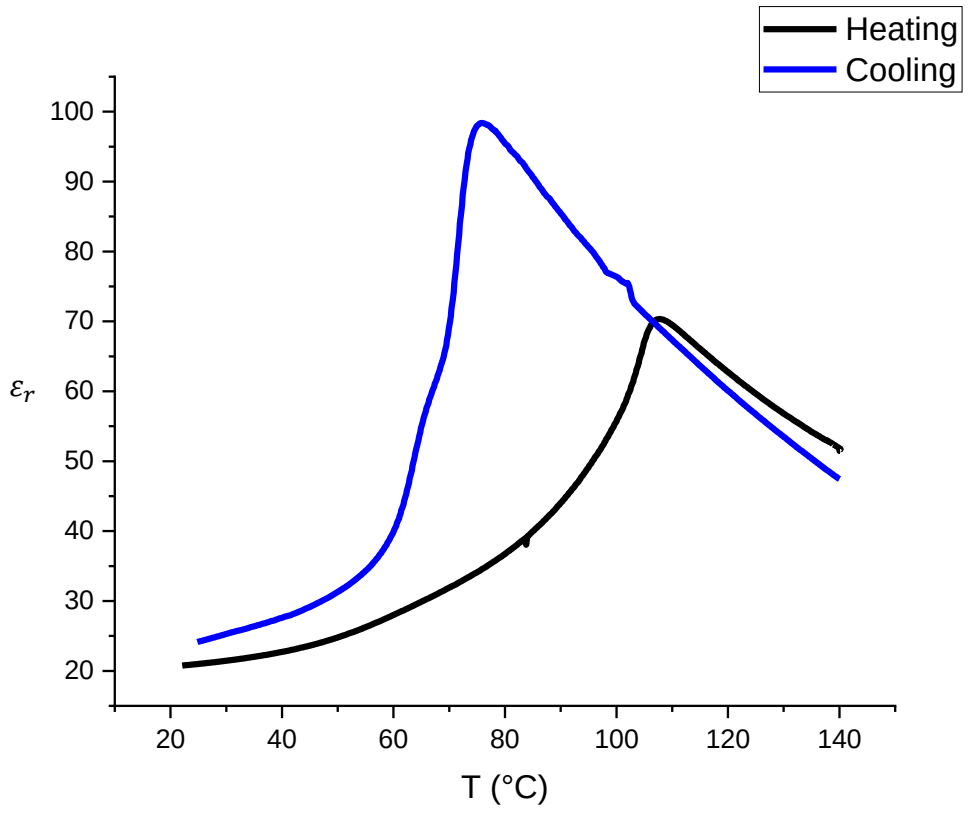

Figure 37-phase transitions of P(VDF-TrFE)-70:30 mol-% (ferroelectric to paraelectric upon heating and paraelectric to ferroelectric upon cooling)-nanocomposite material 1

5.2 P(VDF-TrFE)-BNT nanocomposite:

5.2.1 Poling of nanoparticle phase:

A nanocomposite material with lead free nanoparticles offers an environmental-friendly as well as biocompatible alternative to the lead-based nanoparticles. However, Lead-based ferroelectrics are still widely used because they exhibit superior dielectric, pyroelectric and piezoelectric properties.

The same measurements performed for nanocomposite material 1 were also performed for nanocomposite material 2, which is composed of P(VDF-TrFE) matrix material and bismuth sodium titanite nanoparticles (figure 38).

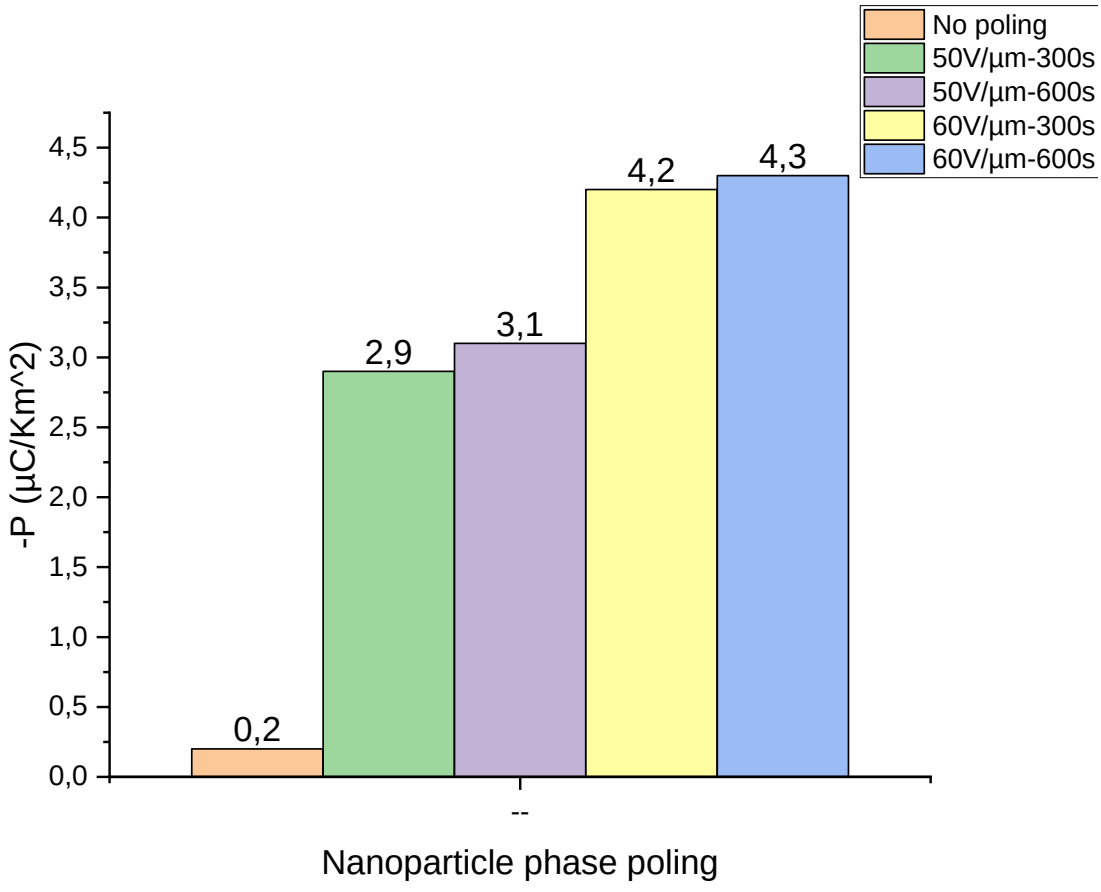

Figure 38-Bismuth Sodium Titanite nanoparticle phase poling investigated for different poling fields and poling times

The pyroelectric coefficient for an unpoled state is 0.2 μC/Km^2. Poling the sample at 50 V/μm for 300 s results in a measured pyroelectric coefficient of 2.9 μC/Km^2. Increasing the poling time to 600 s increased the measured pyroelectric signal to 3.1 μC/Km^2. Increasing the poling field to 60 V/μm and poling the sample for 300 s results in a measured pyroelectric coefficient of 4.2 μC/Km^2. Finally, Increasing the poling time to 600 s while maintaining the poling field at 60 V/μm, yielded a signal of 4.3 μC/Km^2. These results show a minimal change in the measured pyroelectric activity in response to varying poling times. However, a higher influence of the poling field on the measured pyroelectric signal is observed. Again, poling fields below the polymer's coercive field did not allow successful poling of the nanoparticle phase.

5.2.2 Poling of polymer matrix phase:

At an AC poling field of 90 V/µm, the P(VDF-TrFE) polymer has a spontaneous displacement of 64 mC/m^2 and a remnant displacement of 58 mC/m^2. The measured spontaneous and remnant displacement is higher than that obtained for P(VDF-TrFE)-PT nanocomposite. Moreover, It can be observed that the coercive field is around 40 V/µm, which means the dispersed nanoparticles have reduced the polymer's coercive field (figure 39).

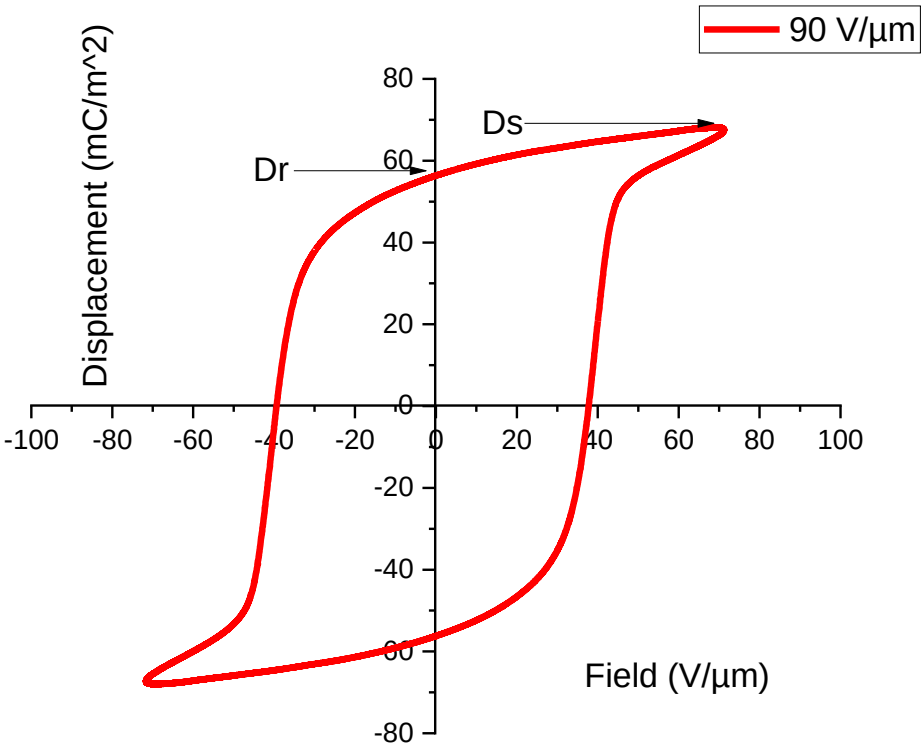

Figure 39- D-E hysteresis obtained for P(VDF-TrFE) matrix phase from AC poling

5.2.3 Pyroelectric signal cancellation:

As for nanocomposite material 1, Both constituents of nanocomposite material 2 possess a negative pyroelectric coefficient. This means that antiparallel poling of both phases eliminates the pyroelectric effect and thus temperature sensitivity (figure 40).

The pyroelectric coefficient for an unpoled state is measured at 0.2 µC/Km^2. After poling the nanoparticle phase, the maximum obtained pyroelectric coefficient is 4.3 µC/Km^2. Antiparallel poling of the matrix phase is done as a consecutive step. The matrix is poled at a field of 40 V/µm and the resultant pyroelectric coefficient drops to 2.7 µC/Km^2. Increasing the poling field up to 45 V/µm, the pyroelectric coefficient is measured at 2.3 µC/Km^2. At 50 V/ µm, the coefficient is measured at 2 µC/Km^2. Further increase of the matrix poling field to 55 V/µm results in a measured pyroelectric coefficient of 0.4 µC/Km^2. Finally, at 60 V/µm, the pyroelectric signal is reduced to 0.06 µC/Km^2.

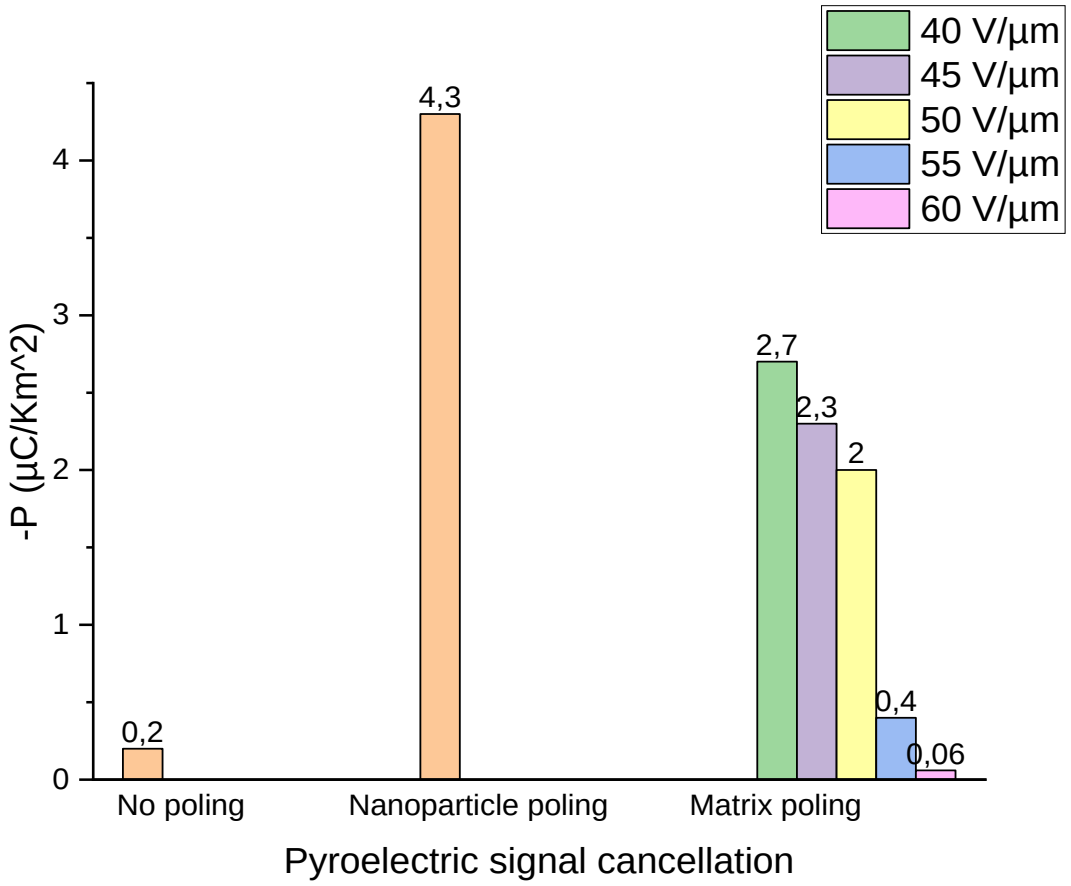

Figure 40-pyroelectric signal cancellation is done by poling the BNT nanoparticle phase and then poling the matrix opposite in direction

5.2.4 Piezoelectric signal cancellation:

To eliminate piezoelectric contributions for nanocomposite material 2, again parallel poling of the nanocomposite's phases is performed. The polymer is characterized by a negative piezoelectric coefficient, and the Bismuth sodium titanite particles, similar to lead titanite nanoparticles, have a positive piezoelectric coefficient (figure 41).

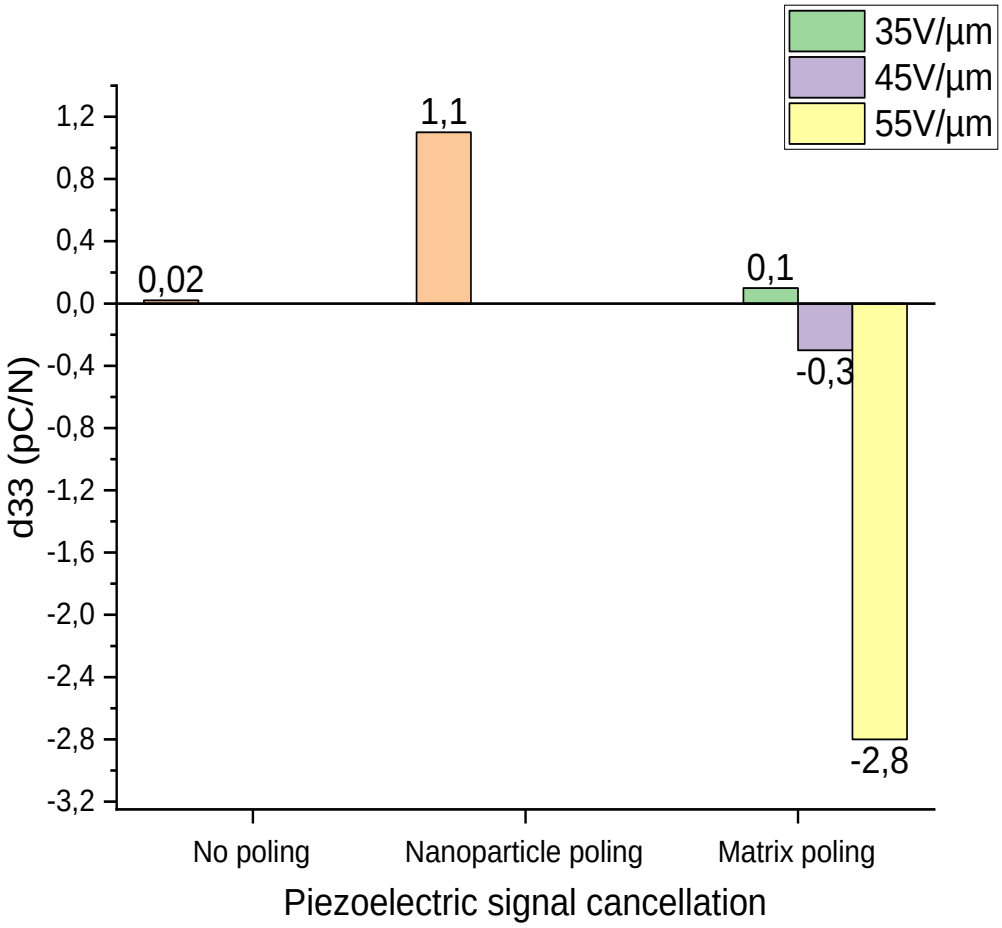

Figure 41-piezoelectric signal cancellation is done by poling the BNT nanoparticle phase and then poling the matrix in the same direction

For an unpoled state, the measured d_{33} coefficient is 0.02 pC/N. From poling of the nanoparticle phase, the measured d_{33} coefficient is measured at 1.1 pC/N. The piezoelectric coefficient drops to 0.1 pC/N when matrix poling was performed at 35 V/µm. further increase of the matrix poling field to 45 V/mm results in a measured d_{33} signal of -0.3 pC/N, indicating that a piezoelectric signal from the polymer phase is obtained. At 55 V/µm, the d_{33} coefficient is measured at -2.8 pC/N.

5.2.5 Ferroelectric-paraelectric phase transition:

Observing the ferroelectric to paraelectric phase transition and vice versa for this nanocomposite material is performed in the same way as for nanocomposite material 1. The dielectric constant increases from 13 (20 for nanocomposite material 1) as the temperature increases, however the maximum measured dielectric constant of 52 upon heating is lower than that of nanocomposite material 1, which is 70. Since the same matrix material is used for both nanocomposites, the Curie temperature of the matrix phase for a heating cycle occurs at 107°C. While cooling, the paraelectric to ferroelectric phase transition occurs at 75°C (figure 42).

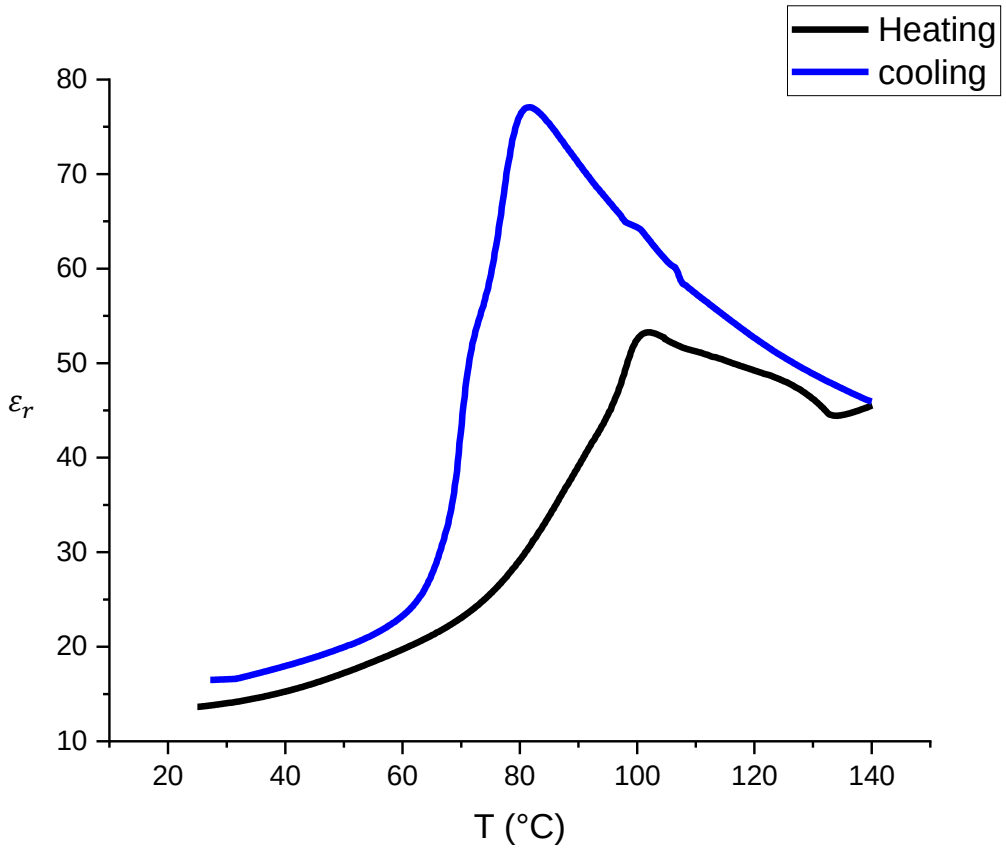

Figure 42-phase transitions of P(VDF-TrFE)-70:30 mol-% (ferroelectric to paraelectric upon heating and paraelectric to ferroelectric upon cooling)-nanocomposite material 2

5.3 Comparison between both nanocomposites:

Table 6 gives a comparison between nanocomposite material 1 and 2. The pyroelectric coefficient of material 1 (P(VDF-TrFE)-PT) is measured at 11.9 µC/Km^2 after poling the nanoparticle phase. In comparison, the pyroelectric coefficient of material 2 (P(VDF-TrFE)-BNT) is measured at 4.3 µC/Km^2 after poling the nanocomposite phase. Therefore, a matrix poling field of 90 V/mm is required for nanocomposite material 1, while nanocomposite material 2 requires a matrix poling field of 60 V/mm for signal compensation.

For the piezoelectric signal cancellation, the nanoparticle phase of nanocomposite material 1 had a d_{33} coefficient of 2.6 pC/N after poling. In comparison to 1.1 pC/N for nanocomposite material 2. Piezoelectric signal compensation occurs at 60 V/mm for nanocomposite material 1, while nanocomposite material 2 requires a matrix poling field of 35 V/mm, which is below the polymer's coercive field.

		$PbTiO_3$ (PT) based nanocomposite	$BiNaTiO_3$ (BNT) based nanocomposite
Pyroelectric signal	Nanoparticle phase	-p=11.9µC/Km2	-p=4.3µC/Km2
	Signal compensation (copolymer)	E=90V/µm	E=60V/µm
Piezoelectric signal	Nanoparticle phase	d33=2.6pC/N	d33=1.1pC/N
	Signal compensation (copolymer)	E=60V/µm	E=35V/µm

Table 8- comparison between nanocomposite material 1 and 2

6. Conclusion:

Ferroelectric nanocomposites composed of PVDF copolymers and ceramic nanoparticles utilizes both pyroelectric and piezoelectric activity suitable for temperature and pressure sensing applications. Unlike single phase ferroelectric PVDF copolymers, which experience simultaneous pyroelectric and piezoelectric activity, the tailored nanocomposite material allows selective enhancement and cancellation of both properties, which leads to selective pressure or temperature sensing.

Two nanocomposite materials are prepared using cost effective screen-printing technique. The 1st material presented is composed of P(VDF-TrFE) 70:30 mol-% matrix phase and PbTiO3 nanoparticles added at 20 vol-%. The 2nd nanocomposite material presented offers a lead-free substitute for the nanoparticle phase and therefore is composed of the same matrix material but instead, BiNaTiO3 nanoparticles are used as a filler phase.

Poling of the nanocomposite constituents was performed, starting with high temperature DC poling of the nanoparticle phase, followed by AC poling of the matrix phase at room temperature. DC poling of the nanoparticle phase depends on the poling field as well as the poling time. Therefore, these two parameters were investigated for both nanocomposites. This was performed by measuring the pyroelectric coefficient of the nanoparticle phase. Lead Titanite nanoparticles exhibited higher pyroelectric response in comparison to Bismuth Sodium Titanite nanoparticles. However, SEM images of P(VDF-TrFE)-BNT nanocomposite showed low nanoparticle density, which might indicate that the BNT content is lower than 20 vol-%. D-E loops obtained for the copolymer matrix phase show that P(VDF-TrFE)-PT nanocomposite shows lower remnant polarization compared to P(VDF-TrFE)-BNT nanocomposite.

Pyroelectric signal cancellation was done by antiparallel poling of the matrix phase with respect to the nanoparticle phase. This translates to reversed polarization direction of the matrix phase with respect to the nanoparticle phase. The pyroelectric coefficient measured for the poled nanoparticle phase was compensated for by a matrix poling field of 90V/µm for the P(VDF-TrFE)-PT nanocomposite. However, for the P(VDF-TrFE)-BNT nanocomposite, a matrix poling field of 60 V/µm was required. For the piezoelectric signal cancellation, parallel poling of the matrix phase with respect to the nanoparticle phase is performed. The piezoelectric coefficient d_{33} is 2.6pC/N for the P(VDF-TrFE)-PT nanocomposite, after poling the nanoparticle phase. However, P(VDF-TrFE)-BNT nanocomposite had a piezoelectric coefficient of 1.1pC/N, after poling the nanoparticle phase. A matrix poling field of 60 V/µm was sufficient to reduce the measured piezoelectric coefficient to 0.14 pC/N for the P(VDF-

TrFE)-PT nanocomposite. However, an even lower poling field was required to cancel the piezoelectric coefficient of the P(VDF-TrFE)-BNT nanocomposite.

6.1 Limitations:

During the course of this thesis, several limitations and issues were present:

1. For starters, producing high quality films with uniform thickness still requires more optimization. High quality films would be characterized by good electrode-nanocomposite adhesion, uniform thickness of printed layer, control over thickness of printed layer and contaminant free printed films.
2. Uniform suspension of nanoparticles inside the matrix phase is a crucial step to avoid inhomogeneous field distributions, which will lead to electrical breakdown of the films during poling. It has been observed that nanoparticle agglomerations form when the nanocomposite ink is stored for few months. This issue was not present in freshly delivered nanocomposite ink.
3. SEM cross sectional images of P(VDF-TrFE)-BNT shows low nanoparticle concentration compared to P(VDF-TrFE)-PT cross sectional images, which might explain why the measured pyroelectric and piezoelectric coefficients after poling the nanoparticle phase were relatively low for the P(VDF-TrFE)-BNT nanocomposite.
4. High temperature poling of the nanoparticle phase was performed on a heat plate without accurate control over the temperature, which did not allow investigation of temperature effect on poling the nanoparticle phase and the resultant pyroelectric and piezoelectric signals.
5. Proper contacting of the samples inside the pyroelectric and piezoelectric setups was an issue, which might influence the measured signals. Signal noise might have an influence on the measured pyroelectric and piezoelectric coefficients, given that the generated charge from the nanoparticle phase is relatively low (around 2 nC for pyroelectric signal and few pC for the piezoelectric signal).

References

1. Kasap, S. (2002). *Piezoelectric Materials and Devices* (Vol. 1). https://doi.org/10.1201/b12709
2. West, R. (1999) *Basic Solid State Chemistry Anthony* 2nd edn.
3. Fundamentals of Piezoelectricity. (n.d.). https://doi.org/10.1007/1-84628-332-9_2
4. https://www.slideshare.net/tufdaawg/covalent-bonding-chapter-8
5. January, P. (2002). Physics of ferroelectrics What is a ferroelectric ? https://doi.org/10.1016/S1369-7021(11)70300-5
6. Ravikumar, G., & Yakhmi, J. V. (2012). *Functional Materials*. *Functional Materials*. https://doi.org/10.1016/B978-0-12-385142-0.00007-6
7. http://faculty-science.blogspot.com/2010/11/ferroelectricity.html
8. Taylor, P., & Furukawa, T. (2006). Phase Transitions : A Multinational Ferroelectric properties of vinylidene fluoride copolymers, (September 2012), 37–41. https://doi.org/10.1080/01411598908206863
9. Pachmajer, S. (2014). Feasibility study for the observation of the inverse piezoelectric effect by X-ray diffraction, (May).
10. Prateek, Thakur, V. K., & Gupta, R. K. (2016). Recent Progress on Ferroelectric Polymer-Based Nanocomposites for High Energy Density Capacitors: Synthesis, Dielectric Properties, and Future Aspects. *Chemical Reviews*, *116*(7), 4260–4317. https://doi.org/10.1021/acs.chemrev.5b00495
11. https://mercy.digication.com/physics2_project/IDK_Yet
12. Zirkl, M. (2007). Martin Zirkl Herstellung und Charakterisierung von ferroelektrischen Polymer-Dünnfilmen und ihre Anwendung in integrierten organischen Infrarotsensoren Dissertation an der Naturwissenschaftlichen Fakultät der Karl-Franzens-Universität Graz.
13. Nanocomposite. (2012). *Mt9100*, 1–36.
14. Khan, W. A. (2016). Polymer nanocomposites–synthesis techniques, classification and properties. *Science and Applications of Tailored Nanostructures, One Central Press*, 50–67.
15. https://www.slideshare.net/TARIQISLAM11/nanoparticle-synthesis-69950600
16. Micjan, M., Nevrela, J., Novota, M., Flickyngerova, S., Juhasz, P., Uhrik, J., … Weis, M. (2014). Ferroelectric polymer films for flexible memory devices, 93–96. http://doi.org/10.1109/ASDAM.2014.6998654

17. Capacitors, A. F. (2016). operating in ultra-high frequency, 2–5.
18. Kim, S., Towfeeq, I., Bayram, F., Khan, D., & Koley, G. (2016). Highly Flexible P (VDF-TrFE) Film-Based Piezoelectric Self-Powered Energy Harvester, *1*, 479–481.
19. Hannah, S., Uttamchandani, D., & Gleskova, H. (2015). Response of P (VDF-TrFE) Sensor to Force and Temperature, 369–372.
20. Rendl, C., Greindl, P., Haller, M., Zirkl, M., Stadlober, B., & Hartmann, P. (2012). PyzoFlex: Printed Piezoelectric Pressure Sensing Foil. *Proceedings of the 25th Annual ACM Symposium on User Interface Software and Technology - UIST '12*, *1*, 509–518. https://doi.org/10.1145/2380116.2380180
21. https://www.joanneum.at/materials/forschungsbereiche/pyzoflexr/
22. Ploss, B., Ploss, B., Shin, F. G., Chan, H. L. W., & Choy, C. L. (2000). Pyroelectric or piezoelectric compensated ferroelectric composites. *Applied Physics Letters*, *76*(19), 2776–2778. https://doi.org/10.1063/1.126472
23. Ploss, B., Ng, W., Chan, H. L., Ploss, B., & Choy, C. (2001). Poling study of PZT / P (VDF ± TrFE) composites, *61*, 957–962.
24. Ploss, B., Ploss, B., Shin, F. G., Choy, C. L., Hom, H., & Kong, H. (2001). PT/PVDF-TrFE 0-3 Composites, 301–304.
25. B. Stadlober, *Printed Pyroelectric Sensors - A review*, Applied Physics Review, accepted (2018)
26. Nair, N. (2017). Nikhil Nair Screen / Stencil printing of flexible polymer / composite based piezoelectric material for haptic feedback and ultrasound applications Screen / stencil printing of flexible polymer / composite based piezoelectric material for haptic feedback a, 14–29.
27. Søndergaard, R. R., Hösel, M., & Krebs, F. C. (2013). Roll-to-Roll fabrication of large area functional organic materials. *Journal of Polymer Science, Part B: Polymer Physics*, *51*(1), 16–34. https://doi.org/10.1002/polb.23192
28. Höesel, M. (2013). *Large-Scale Roll-to-Roll Fabrication of Organic Solar Cells for Energy Production.*
29. https://www.saxoprint.co.uk/blog/screen-printing-process/
30. Ammattikorkeakoulu, M. (2016). Seripainettujen elektrodien käyttö biosenso- reissa.
31. Information, P. (n.d.). Melinex, (2).
32. World, C., & City, H. (1982). V). 4., (81098168), 2–3.
33. Pe, D. (n.d.). Dupont ™ pe828.

34. Noliac. (2012). Piezo basics. *Textile Research Journal*, *3*(1), 1–19. Retrieved from http://www.noliac.com/fileadmin/user_upload/documents/Tutorials/Tutorials_Piezo_basics.pdf
35. I. B. Misirlioglu, M. B. Okatan, & S. P. Alpay (2010). Asymmetric hysteresis loops and smearing of the dielectric anomaly at the transition temperature due to space charges in ferroelectric thin films
36. Dietze, M., & Es-Souni, M. (2008). Structural and functional properties of screen-printed PZT-PVDF-TrFE composites. *Sensors and Actuators, A: Physical*, *143*(2), 329–334. https://doi.org/10.1016/j.sna.2007.11.016
37. Krause, M., Graz, I., Bauer-Gogonea, S., Bauer, S., Ploss, B., Zirkl, M., … Helbig, U. (2011). PbTiO3-P(VDF-TrFE) – Nanocomposites for Pressure and Temperature Sensitive Skin. Ferroelectrics, *419*(January 2012), 23–27. https://doi.org/10.1080/00150193.2011.594412
38. Lam, K. H., Wang, X., & Chan, H. L. W. (2005). Piezoelectric and pyroelectric properties of (Bi0.5Na 0.5)0.94Ba0.06TiO3/P(VDF-TrFE) 0-3 composites. *Composites Part A: Applied Science and Manufacturing*, *36*(11), 1595–1599. https://doi.org/10.1016/j.compositesa.2005.03.007
39. Ploss, B., Ploss, B., Shin, F. G., Choy, C. L., Hom, H., & Kong, H. (2001). PT/PVDF-TrFE 0-3 Composites, 301–304.
40. Siponkoski, T., Nelo, M., Palosaari, J., Peräntie, J., Sobocinski, M., Juuti, J., & Jantunen, H. (2015). Electromechanical properties of PZT/P(VDF-TrFE) composite ink printed on a flexible organic substrate. *Composites Part B: Engineering*, *80*, 217–222. https://doi.org/10.1016/j.compositesb.2015.05.018
41. Uchino, K. (2010). *Advanced Piezoelectric Materials*. *Woodhead Publishing Series in Electronic and Optical Materials*(Vol.9). https://doi.org/10.1533/9781845699758.frontmatter
42. Kour, P., Kumar, P., Sinha, S. K., & Kar, M. (2015). Study of dielectric and impedance spectroscopy of La substituted nanocrystalline Pb(Zr0.52Ti0.48)O3 ceramics. *Journal of Materials Science: Materials in Electronics*, *26*(3), 1304–1310. https://doi.org/10.1007/s10854-014-2538-2
43. *Piezotech electro-active polymers*, http://www.piezotech.eu/en/Products/Powders (2017)

44. http://www.te.com/usa-en/products/brands/meas.html?tab=pgp-story (2017)
45. H. Meixner, *IR-sensor-arrays based on PVDF*, Ferroelectrics 115, 279 (1991); H. Meixner and G. Mader, *Pyroelektrische IR-Detektoren auf Polymerbasis*, Physik i. u. Zeit 21, 210 (1990)
46. rp acoustics, *PVDF hydrophones*, http://www.rpacoustics.de/english/PVDF_Hydrophone.htm/ (2017)
47. AVL Ditest, https://www.avlditest.com/index.php/en/startpage-en.html (2017)
48. Cold Gold, http://contactmicrophones.com/ (2017)
49. fils, film speaker technology, http://www.fils.co.kr/ (2017)
50. Piezotech Arkema, *PVDF gauges*, http://www.piezotech.eu/en/Products/Devices/ (2017)
51. A. J. Tuzzolino, *Applications of PVDF dust sensor systems in space*, Adv. Res. Space 17, 121 (1995)
52. L. Seminara et al., *Electromechanical characterization of piezoelectric PVDF polymer films for tactile sensors in robotics applications*, Sensors and Actuators A: Physical, 169(1), 49 (2011)
53. Piezoech Arkema,*Piezotech electroactive polymers*, http://www.piezotech.eu/en/Products/Powders (2017)
54. Solvay,http://www.solvay.com/en/markets-and-products/featured-products/solvene.html (2017)
55. M. Dietze, et al., *Thick film polymer-ceramic composites for pyroelectric applications*; J. Appl. Phys. 101, 054113 (2007)
56. T. Sekine et al., *Fully printed and flexible ferroelectric capacitors based on a ferroelectric polymer for pressure detection*, Jpn. J.Appl. Phys. 55, 10TA18 (2016)
57. S. K. Khaitan, *Design Techniques and Applications of Cyber Physical Systems: A Survey*, IEEE Systems Journal 9, 350 (2015)
58. O. Pabst et al., *Inkjet printed micropump actuator based on piezoelectric polymers: Device performance and morphology studies*, Organic Electronics 15, 3306 (2015)
59. S. Wagle, et al., *Ultrasonic properties of all-printed piezoelectric polymer transducers*, Appl. Phys. Lett 103, 262902 (2013)
60. C. Hübler et al. , *Fully mass printed loudspeakers on paper*, Org. Electr. 13, 2290 (2013)

Appendix

DIAdem code for D-E hystereis loop:

```
Dim SourceChannel, _

NewChannelCopy, getlastelementIntegration, sMessungChannels, _

dTimeStart, dTimeEnd, dOffset, dEndValue, dgetOffset, dgetEndValue,
dChnEventResultList, dgetCoerciveField, _

sPath, sFileName, sNewFile, iMaxGroups, iIndex, iSummaryGroupIndex, Index,_

dMeasurementTime, dCharge, dkValues, dCalcMeasureTime, dCalcCharge, dCalcThickness,
dcalcKValue, _

InputFrequ, dt, iIndexTime, sFormula, aValues(5), aSymbol(5), ChFrequ, Area,
dDisplacement, _

dgetDisplacement, get2500Displacement, dCoerciveField, dgetCalcThickness, CFS, Treshold,
Periods, SamplesPeriod, get2500, DeleteValues , SamplesTotal


'Get FilePath for saving analyzed data

sPath = DataReadPath

sFileName = Data.Root.Name

sNewFile = sPath & sFileName & "_analyzed.tdms"

iMaxGroups=0

iIndex = 1

aSymbol(1) = "A"

aSymbol(2) = "B"

aSymbol(3) = "C"

aSymbol(4) = "D"

Area = 0


'User input

Area = InputBox("Area in cm² ( x,x ):", "Define Sensor Area", 0)

'MsgBox(Area)

aValues(3) = 0.0001 * Area


'Schichtdickenberechnung auf Eingabe Coercive Field Strength
```

```
CFS = InputBox("Coercive Field Strength in V/µm:", "Material dependent Coercive Field Strength", 50)
'MsgBox(Area)

'Abfrage Peak Treshold
'Treshold = InputBox("Peak Treshold:", "Define Treshold", 8)

'GroupCount
iMaxGroups = GroupCount
iSummaryGroupIndex = iMaxGroups + 1

'Add Summary Group and Channels
Call Data.Root.ChannelGroups.Add("Summary", iSummaryGroupIndex).Activate()

sMessungChannels = ChnAlloc("Messung", iMaxGroups, 1,DataTypeString,"Text")
dOffset = ChnAlloc("Offset", iMaxGroups, 1)
dEndValue = ChnAlloc("EndValue", iMaxGroups, 1)
dCharge = ChnAlloc("Charge", iMaxGroups, 1)
dDisplacement = ChnAlloc("Displacement", iMaxGroups, 1)
Call ChnPropSet("Displacement", "unit_string", "mC/m2")
dCoerciveField = ChnAlloc("Coercive Field", iMaxGroups, 1)
Call ChnPropSet("Coercive Field", "unit_string", "V")
dCalcThickness = ChnAlloc("Calculated Thickness", iMaxGroups, 1)
Call ChnPropSet("Calculated Thickness", "unit_string", "µm")

'Analyze Data
for iIndex = 1 To iMaxGroups
  Call Data.Root.ChannelGroups(iIndex).Activate() 'Got to actual group

  SamplesTotal = Data.Root.ActiveChannelGroup.Properties("Samples__").Value
  SamplesTotal = Val(SamplesTotal)
```

```
  Periods = Data.Root.ActiveChannelGroup.Properties("Periods__").Value 'Berechnung der Zeilenanzahl
  Periods = Val(Periods)
  'MsgBox(Periods)

  'Periodenkorrektur fällt ab 16.02.2017 weg (da korrigiert, oder auch nicht)
  Periods = Periods-0.5 'Korrektur der aufgerundeten Periodenzahl (letzte Halbwelle fehlt)

  SamplesPeriod = SamplesTotal/Periods

  ChFrequ = Data.Root.ActiveChannelGroup.Properties("Frequency__Hz_").Value
  ChFrequ = Replace(ChFrequ,",",".")
  ChFrequ = Val(ChFrequ)
  dt = 1/ChFrequ
  Call ChnLinGen("/Time",0,dt,SamplesPeriod,"") 'generieren des Zeitkanals für Periode

  DeleteValues = SamplesTotal - SamplesPeriod
  Call DataBlDel ("["& iIndex &"]/HV Monitor Voltage", 1, DeleteValues)
  Call DataBlDel ("["& iIndex &"]/HV Monitor Current", 1, DeleteValues)

  'alternative Formeln zum Abschneiden von Überschlägen
  'Index = 1
  'Do While (Index > 0)
    'Index = FIND("Ch(""["& iIndex &"]/HV Monitor Current"")>10") 'Positiver Bereich zum Abschneiden von Durchbrüchen
    'if (Index > 0) Then
    'chd(Index, "["& iIndex &"]/HV Monitor Current") = 0
    'end if
  'Loop

  'Index = 1
```

```
  'Do While (Index > 0)
    'Index = FIND("Ch(""["& iIndex &"]/HV Monitor Current"")<-10") 'Negativer Bereich zum Abschneiden
    'if (Index > 0) Then
    'chd(Index, "["& iIndex &"]/HV Monitor Current") = 0
    'end if
  'Loop

  SourceChannel = "["& iIndex &"]/HV Monitor Current"
  NewChannelCopy = ChnAlloc("HV Monitor Current Copy", ChnLength(SourceChannel), 1, ChnValueDataType(SourceChannel))
  Call ChnCopy(SourceChannel , NewChannelCopy(0))
  Call Calculate("Ch(""["& iIndex &"]/HV Monitor Current Copy"")=Abs(Ch(""["& iIndex &"]/HV Monitor Current Copy""))",NULL,NULL,"")
  Call ChnIntegrate("["& iIndex &"]/Time","["& iIndex &"]/HV Monitor Current","/Integrated","TrapezoidalRule",0,0,0)
  Call ChnIntegrate("["& iIndex &"]/Time","["& iIndex &"]/HV Monitor Current Copy","/abs Integrated","TrapezoidalRule",0,0,0)

  getlastelementIntegration = ChnPropGet("["& iIndex &"]/Integrated", "length")

  dgetEndValue = Data.Root.ActiveChannelGroup.Channels("abs Integrated").Values(getlastelementIntegration)
  dgetOffset = Data.Root.ActiveChannelGroup.Channels("Integrated").Values(getlastelementIntegration)

  Call Data.Root.ChannelGroups(iIndex).Channels.Add("Offset corrected",DataTypeFloat64,3) 'Add New Channel

  Set aValues(1) = Data.GetChannel("["& iIndex &"]/HV Monitor Current")
  aValues(2) = dgetOffset*ChFrequ

  sFormula = "Ch(""["& iIndex &"]/Offset corrected"") = A - B"
  Call Calculate (sFormula, aSymbol, aValues)
```

```
  Call ChnIntegrate("["& iIndex &"]/Time","["& iIndex &"]/Offset
corrected","/IntegratedTime","TrapezoidalRule",0,0,0)


  Set aValues(1) = Data.GetChannel("["& iIndex &"]/IntegratedTime")

  sFormula = "Ch(""["& iIndex &"]/Displacement"") = A / C"

  Call Calculate (sFormula, aSymbol, aValues)


  get2500 = SamplesPeriod/2

  'MsgBox(get2500)


  'get2500Displacement = ChV(2500,"["& iIndex &"]/Displacement") 'Variabler Wert ->
Muss angepasst werden:

  get2500Displacement = ChV(get2500,"["& iIndex &"]/Displacement")

  get2500Displacement =get2500Displacement * 0.5


  aValues(4) = get2500Displacement

  Set aValues(1) = Data.GetChannel("["& iIndex &"]/Displacement")

  sFormula = "Ch(""["& iIndex &"]/Displacement"") = A - D"

  Call Calculate (sFormula, aSymbol, aValues)


  ' EVENT DETECTION für Coercive Field


    ChnEventResultList = Null

    ChnEventResultList = ChnEventDetectionWindow ("["& iIndex &"]/HV Monitor
Voltage", "["& iIndex &"]/Displacement", -2, 2, 0, 0)

    Call ChnEventCreateStatusChn("["& iIndex &"]/EventStatus", ChnEventResultList, "["&
iIndex &"]/Displacement", 0, 1)

    Call ChnMul("["& iIndex &"]/EventStatus","["& iIndex &"]/HV Monitor
Voltage","/Multiplied")

    Call Calculate("Ch(""["& iIndex &"]/Multiplied"")=Abs(Ch(""["& iIndex
&"]/Multiplied""))")

    Call Calculate("Ch(""["& iIndex &"]/Multiplied"")=(Ch(""["& iIndex
&"]/Multiplied"")+CTNV(Ch(""["& iIndex &"]/Multiplied"")=0))")
```

```
    StatArithMean = Null
    Call StatBlockCalc("Channel", "1-", "["& iIndex &"]/Multiplied")
    dgetCoerciveField = 1000*StatArithMean
    'MsgBox(dgetCoerciveField)

    dgetCalcThickness = dgetCoerciveField/CFS
    'MsgBox(dCalcThickness)

  Call Data.Root.ChannelGroups(iSummaryGroupIndex).Activate() 'Call Summary Group

  'copy Values in Summary table
  ChT(iIndex,sMessungChannels(0)) = "M" & iIndex
  ChD(iIndex,dOffset(0)) = dgetOffset
  ChD(iIndex,dEndValue(0)) = dgetEndValue

  dCalcCharge = abs(dgetOffset)+abs(dgetEndValue)
  ChD(iIndex,dCharge(0)) = dcalcCharge
  ChD(iIndex,dDisplacement(0)) = abs(get2500Displacement)
  ChD(iIndex,dCoerciveField(0)) = dgetCoerciveField
  ChD(iIndex,dCalcThickness(0)) = dgetCalcThickness

Call DeleteData

Next

Call DataFileSave(sNewFile,"TDMS")

Sub DeleteData() 'Delete Data
  'Call Data.Root.ChannelGroups(iIndex).Channels.Remove("HV Monitor Voltage")
  'Call Data.Root.ChannelGroups(iIndex).Channels.Remove("HV Monitor Current")
```

```
Call Data.Root.ChannelGroups(iIndex).Channels.Remove("HV Modulation Signal Set")
Call Data.Root.ChannelGroups(iIndex).Channels.Remove("HV Monitor Current Copy")
Call Data.Root.ChannelGroups(iIndex).Channels.Remove("Integrated")
Call Data.Root.ChannelGroups(iIndex).Channels.Remove("abs Integrated")
'Call Data.Root.ChannelGroups(iIndex).Channels.Remove("Offset corrected")
Call Data.Root.ChannelGroups(iIndex).Channels.Remove("IntegratedTime")
'Call Data.Root.ChannelGroups(iIndex).Channels.Remove("Time")
Call Data.Root.ChannelGroups(iIndex).Channels.Remove("EventStatus")
'Call Data.Root.ChannelGroups(iIndex).Channels.Remove("Multiplied")
'folgende Löschen
Call Data.Root.ChannelGroups(iIndex).Channels.Remove("ArithmeticMean")
Call Data.Root.ChannelGroups(iIndex).Channels.Remove("Sum")

End Sub
```

MATLAB code for piezoelectric coefficient evaluation:

```
%% load data
```

```
clear all
Rconv = -9.984e6; %resistance [Ohm] for I/U conversion
Cconv = 10e-9; %capacitance [F] for I/Q conversion; Q = C*U

default_Filefolder = 'D:\ARBEITSORDNER\PYZOFLEX Charakterisierung';
%default_Filefolder = 'D:\ARBEITSORDNER\PYZOFLEX Charakterisierung\HeavyStamp\Taher_06122017\15.02';
%default_Filefolder = 'D:\ARBEITSORDNER\PROJEKTE - laufend\SELF-PoSH_ARBEITSORDNER\WP5_SMApplication_Poling_Sensor Evaluation\HeavySTamp';

%[ Ch File_folder File_name ] = ReadDXD( default_Filefolder, [] ); % load DXD file containing poling current and voltage in channels 1 and 2

[ File_name, File_folder, filterindex] = uigetfile(strcat(default_Filefolder, '\', '*.dxd;*.tdms'),'Select a DXD file');

if contains(File_name, '.dxd')
   [ Ch File_folder File_name ] = ReadDXD( File_folder, File_name, [] );

   stype = 'DEWESOFT';

   qans = questdlg('Define measurement type:',...
            'Measurement type', 'I/U ext.', 'I/Q ext.', 'I/Q int.', 'I/U ext.');
   % select data channels to evaluate
   switch qans
      case 'I/U ext.'
         %iforce = 2;
         %isens = 5;
         iforce = 2;
         isens = 4;
         f_conv = 1e-9; %unit conversion factor
         senstype = 'I';
```

```
        case 'I/Q ext.'
            iforce = 2;
            isens = 1;
            f_conv = 1e-9; %unit conversion factor
            senstype = 'Qext';

        case 'I/Q int.'
            iforce = 2;
            isens = 1;
            f_conv = 1e-9; %unit conversion factor
            senstype = 'Qint';

        otherwise
            isens = 1;
            iforce = 2;
            f_conv = 1e-9; %unit conversion factor
            senstype = 'I';
    end

    forceT_raw = Ch{iforce}.timestamp;
    force_raw = Ch{iforce}.data;
    sensT_raw = Ch{isens}.timestamp;
    sens_raw = Ch{isens}.data*f_conv;
    Srate = Ch{1}.srate;

elseif contains(File_name, '.tdms')
    % load TDMS file
    stype = 'NI';
    %isel = [1 2 5 6];
    isel = [20 21 24 25];
```

```
    f_conv = 1; % %unit conversion factor
    [ selCh ] = ReadTDMST ( strcat(File_folder, '\', File_name), isel );

    forceT_raw = selCh{1}.val';
    force_raw = -selCh{2}.val'*f_conv;
    sensT_raw = selCh{3}.val'*f_conv;
    sens_raw = selCh{4}.val';
    Srate = 1/(sensT_raw(2)-sensT_raw(1));
    senstype = 'I';
end

% plot sense data
figure();
plot(sensT_raw, sens_raw);
xlabel('t [s]'); ylabel('sensor signal');
title(sprintf('%s', File_name), 'interpreter', 'none');

% plot force data
figure;
plot(forceT_raw, force_raw);
xlabel('t [s]'); ylabel('force');
title(sprintf('%s', File_name), 'interpreter', 'none');

%% enter evaluation parameters

sprompt = {'Excitation Freqency [Hz]:', 'Time offset:', '# of periods'};
ansprompt = inputdlg( sprompt, 'Enter measuring parameters', 1, {'0.5', '2', '4'} );

if isempty(ansprompt)
else
    f_exc = str2num(ansprompt{1}); % excitation frequency [Hz]
```

```
    t_offset = str2num(ansprompt{2}); % time offset from where to take data
    Nperiods = str2num(ansprompt{3}); % # of periods over which to choose data

end

t_Ioff = 0.5;
iSel = find((sensT_raw>t_offset)&(sensT_raw<(t_offset+Nperiods/f_exc)));
iSel_force = find((forceT_raw>t_offset)&(forceT_raw<(t_offset+Nperiods/f_exc)));
iSel_offset = find((sensT_raw<(t_Ioff+sensT_raw(10))) & (sensT_raw > sensT_raw(10)));
sens_raw = sens_raw - mean(sens_raw(iSel_offset)); % remove idle current offset

sensT = sensT_raw(iSel)';
force = force_raw(iSel_force)';
forceT = forceT_raw(iSel_force)';

tmeasure = sensT(end)-sensT(1);
tsample = tmeasure/length(sensT); % sample period
tsample_f = (forceT(end)-forceT(1))/length(forceT);

% filter data

% ##################################
% ## SIGNAL FILTERING SETTINGS ####
% ##################################

% main noise peaks to be suppressed:
switch stype
    case 'DEWESOFT'
    % filter settings [Hz]
    f_cutoff = [ 0 2/tsample ]; % cutoff frequencies
```

```
    f_peaks = [ 50 ]; % notchfilter frequency
    bw = 2; % band width of peak

    case 'NI'
    f_cutoff = [ 0 1000 ];
    %f_peaks = [ 50 704.4];
    f_peaks = [ 50 ]
    bw = 2;
end

[sens_raw_filtered, sens_raw_fsignal_filtered, f] = notchfilter( sens_raw', sensT_raw',
f_peaks, bw, f_cutoff, 0 );
sens_filtered = sens_raw_filtered(iSel);
% calculate charge data

%Qsens = sens_filtered;
switch senstype
    case 'I'
        %Qsens = cumtrapz(sens_filtered)*tsample; %[C]
        Qsens = cumtrapz(sens_filtered-mean(sens_filtered))*tsample; %[C]

    case 'Qext'
        Qsens = sens .* Cconv; %[C]

    case 'Qint'
        Qsens = sens; %[C]

end

%% Plot data
bpol = -1;
```

```
[fpath fname ext] = fileparts(File_name);

f_FQtime = figure();
yyaxis left;
plot(sensT, bpol*Qsens, '.');
xlabel('t [s]'); ylabel('charge [C]');
yyaxis right;
plot(forceT, -force);
% ax = gca();
% as.YAxis(1).Limits = [0.9*max(bpol*Qsens) 1.1*max(bpol*Qsens)];
% ax.YAxis(2).Limits = ax.YAxis(1).Limits * 1/18e-3;
ylabel('force, -Fz [N]');
title(sprintf('HS meas. of: %s', fname), 'interpreter', 'none');
thisfig = gcf();
Nsavefig = thisfig.Number;

%% extract piezoelectric coefficient
force_threshold = 0.1;

if length(force)<length(Qsens)
   Qsens = interpn(sensT, Qsens, forceT);
elseif length(force)>length(Qsens)
   warning('sampling frequency of Qsens lower than of force');
end

Np = int64(1/(f_exc*tsample_f));

Ndata = 1000; % number of data points extracted per excitation
%N_delta = int64(Np/Ndata);
N_delta = 1;
```

```
% evaluate piezocoefficient per excitation cycle

exc_data = cell(Nperiods,1);

for n=1:Nperiods

    if n*Np <= length(iSel_force)
        Nrange = int64(1+(n-1)*Np):int64(n*Np);
    else
        Nrange = int64(1+(n-1)*Np):length(iSel_force);

    end

    % get force and charge data for selected period and remove offset
    % values
    force_base(n) = min(-force(Nrange));
    Q_base(n) = min(bpol*Qsens(Nrange));

    imax = find(-force(Nrange) > max(-force(Nrange))*force_threshold);

    Qsens_max(n) = max(bpol*Qsens(imax)) - Q_base(n);
    exc_data{n}.Qsens_max = Qsens_max(n);
    force_max(n) = max(-force(imax)) - force_base(n);
    exc_data{n}.force_max = force_max(n);

    exc_data{n}.force = -force(Nrange) - force_base(n); % excitation force, offset reduced
    exc_data{n}.charge = bpol*Qsens(Nrange(1:N_delta:end)) - Q_base(n); % measured
charge, offset reduced
    exc_data{n}.timestamp = forceT(Nrange);

    n_hp1 = int64(length(exc_data{n}.force)/2);
```

```
    f_inc = exc_data{n}.force(1:n_hp1)';
    Q = exc_data{n}.charge(1:n_hp1)';
    ifit = find((f_inc > force_threshold*force_max(n))&(f_inc < (1-
force_threshold)*force_max(n)));

    Q_inc = [ ones(length(ifit), 1) Q(ifit)];
    exc_data{n}.d = -f_inc(ifit) \ Q_inc;

end

%% plot piezoelectric coefficients
f_d33_bar = figure();
hold on;
for n=1:length(exc_data)
    bar(n, abs(exc_data{n}.d(2))*1e12, 'b');
end
xlabel('period #'); ylabel('|d_{33}| (pC/N)');
title(sprintf('HS meas. of: %s', fname), 'interpreter', 'none');

%% Plot charge vs. force
selperiod = 5;
n_hp1 = int64(length(exc_data{selperiod}.force)/2);
n_hp1_Q = int64(length(exc_data{selperiod}.charge)/2);
f_FQfit = figure();
%plot(exc_data{selperiod}.force, exc_data{selperiod}.charge, '.');

hold on;
plot(exc_data{selperiod}.force(1:n_hp1), exc_data{selperiod}.charge(1:n_hp1_Q), '.', 'Color',
'blue');
plot(exc_data{selperiod}.force(n_hp1+1:end), exc_data{selperiod}.charge(n_hp1_Q+1:end),
'.', 'Color', 'green');
```

```
%plot(exc_data{selperiod}.force(1:n_hp1)*1.1, -
exc_data{selperiod}.d(2)*exc_data{selperiod}.force(1:n_hp1)*1.1+exc_data{selperiod}.d(1),
'--', 'Color', 'black');

plot(exc_data{selperiod}.force(1:n_hp1)*1.1, -
exc_data{selperiod}.d(2)*exc_data{selperiod}.force(1:n_hp1)*1.1, '--', 'Color', 'black');

text(exc_data{selperiod}.force_max/2, 5, sprintf('d_{33} = %.1f pC/N', -
exc_data{selperiod}.d(2)*1e3), 'FontSize', 11);

xlabel('force, -Fz [N]'); ylabel('charge [C]');

legend(sprintf('period #%d, F increasing',selperiod), sprintf('period #%d, F
decreasing',selperiod), 'linear fit (inc)', 'Location', 'northwest');

title(sprintf('HS meas. of: %s', fname), 'interpreter', 'none');


%% save figures

if exist('f_FQfit')

   savefig(f_FQfit, strcat(File_folder, '\', fname, '_FQfit_period#', num2str(selperiod), '.fig'));

   saveas(f_FQfit, strcat(File_folder, '\', fname, '_FQfit_period#', num2str(selperiod), '.tif'));

end


if exist('f_d33_bar')

   savefig(f_d33_bar, strcat(File_folder, '\', fname, '_d33bar', '.fig'));

   saveas(f_d33_bar, strcat(File_folder, '\', fname, '_d33bar', '.tif'));

end


if exist('f_FQtime')

   savefig(f_FQtime, strcat(File_folder, '\', fname, '_FQtime', '.fig'));

   saveas(f_FQtime, strcat(File_folder, '\', fname, '_FQtime', '.tif'));

end


%% save data to file


hs_test.fname = fname;

hs_test.ffolder = File_folder;

hs_test.tsample = tsample;
```

```
hs_test.bpol = bpol;
hs_test.f_exc = f_exc;
hs_test.filter = f_peaks;
hs_test.force_threshold = force_threshold;
hs_test.force = force;
hs_test.forceT = forceT;
hs_test.sens = sens;
hs_test.sens_filtered = sens_filtered;
hs_test.Qsens = Qsens;
hs_test.exc_data = exc_data;

filename_mat = strcat(File_folder, fname, '.mat');
filename_fig = strcat(File_folder, fname, '_QFtimeplot', '.fig');

if exist(filename_mat)==2
   boverwrite = questdlg(sprintf('File %s.mat already exists. Overwrite?',fname), 'Save
hs_test', 'Yes', 'No', 'No');
   switch boverwrite
      case 'Yes'
         save(filename_mat, 'hs_test');
      otherwise
   end
else
   save(filename_mat, 'hs_test');
end

if exist(filename_fig)==2
   boverwrite = questdlg('File already exists. Overwrite?', 'Save figure 3', 'Yes', 'No', 'No');
   switch boverwrite
      case 'Yes'
         figure(Nsavefig);
```

```
            savefig(filename_fig);
        otherwise
    end
else
    figure(3);
    savefig(filename_fig);
end

%% Open multiple data files

default_Filefolder = 'D:\ARBEITSORDNER\PYZOFLEX
Charakterisierung\HeavyStamp\Auswertung';

[filename,filefolder]=uigetfile(strcat(default_Filefolder, '\', '*.mat'),'Select a DXD file',
'MultiSelect', 'On');
%%
if ~iscell(filename)
    cfilename = cell(1);
    cfilename{1} = filename;
else
    cfilename = filename;
end

Nmeasure = length(cfilename);
mseries = cell(1, Nmeasure);

Nperiod_exc = 4*ones(1, Nmeasure); % choose which period to take as representive data for
excitation

figure;
hold on;
for i=1:Nmeasure
```

```
    A = open(strcat(filefolder, cfilename{i}));
    mseries{i}.exc_data = A.hs_test.exc_data;
    mseries{i}.name = cfilename{i};
    mseries{i}.tsample = A.hs_test.tsample;
    clear A;

    plot( mseries{i}.exc_data{Nperiod_exc(i)}.force,
mseries{i}.exc_data{Nperiod_exc(i)}.charge );
    idx = strfind(cfilename{i}, 'N');
    sexc_forceNom{i} = replace(cfilename{i}(idx-4:idx), '_', '');

end

hold off;
xlabel('force, -Fz [N]'); ylabel('charge [C]');
legend(sexc_forceNom);
title('generated charge vs. excitation force')

%% plot

iseries = 1;
iperiod = 7;
piezo_extr = 0.01797;
%piezo_extr = 0.01811;
Q_offset_extr = 0.18;
force = mseries{iseries}.exc_data{iperiod}.force;
charge = mseries{iseries}.exc_data{iperiod}.charge;
timestamp = mseries{iseries}.exc_data{iperiod}.timestamp;

imax = find(force > max(force)*0.9);
figure();
```

```
hold on;
plot(timestamp(imax), force(imax)*piezo_extr+Q_offset_extr);
%plot(imax, force(imax)*piezo_extr);
plot(timestamp(imax), charge(imax), '.');
hold off;
xlabel('t [s]'); ylabel('charge [C]');
legend({'F * d_33', 'Q'}, 'interpreter', 'none');
title(sprintf('generated charge vs. excitation force, F_max=%0.0fN',
mseries{iseries}.exc_data{iperiod}.force_max), 'interpreter', 'none');

%% time derivative of force
delta_Q = charge - force*piezo_extr;
dforce = diff(force)/tsample;
figure();
yyaxis left;
plot((1:length(force)-1)*tsample, -dforce);
ylabel('dF/dt [N/s]');
yyaxis right;
plot((1:length(force))*tsample, delta_Q);
xlabel('t [s]'); ylabel('charge [C]');
legend('-dF/dt','\DeltaQ');
title(sprintf('F_max=%0.0fN', mseries{iseries}.exc_data{iperiod}.force_max), 'interpreter',
'none');

%%
%piezo_coeff(n) = (Qsens(imax)./force(imax)); %[pC]
piezo_coeff_mean = mean(Qsens_max./force_max); %[pC]
%piezo_coeff_std = std(piezo_coeff); %[pC]

figure();
yyaxis left;
```

```
plot(sensT(imax), bpol*Qsens(imax), '.');
xlabel('t [s]'); ylabel('charge [C]');
yyaxis right;
plot(forceT(imax), -force(imax));
ax = gca();
ax.YAxis(2).Limits = ax.YAxis(1).Limits * 1/piezo_coeff_mean;
ylabel('force, -Fz [N]');
title(sprintf('HS meas. of: %s', fname), 'interpreter', 'none');

figure();
plot(sensT(imax), piezo_rel(imax), '.');
xlabel('t [s]'); ylabel('Q/F [pC/N]');
title(sprintf('HS meas. of: %s', fname), 'interpreter', 'none');
```